Tomographic PIV in a model of the left ventricle

3D flow past biological and mechanical heart valves

Saaid, Hicham; Voorneveld, Jason; Schinkel, Christiaan; Westenberg, Jos; Gijsen, Frank; Segers, Patrick; Verdonck, Pascal; de Jong, Nico; Kenjeres, Sasa; More Authors

DOI
10.1016/j.jbiomech.2019.04.024

Publication date
2019

Document Version
Accepted author manuscript

Published in
Journal of Biomechanics

Citation (APA)
Saaid, H., Voorneveld, J., Schinkel, C., Westenberg, J., Gijsen, F., Segers, P., Verdonck, P., de Jong, N., Kenjeres, S., & More Authors (2019). Tomographic PIV in a model of the left ventricle: 3D flow past biological and mechanical heart valves. *Journal of Biomechanics*, *90*, 40-49. https://doi.org/10.1016/j.jbiomech.2019.04.024

Elsevier Editorial System(tm) for Journal of Biomechanics

Manuscript Draft

Manuscript Number: BM-D-18-01151R1

Title: Tomographic PIV in a Model of the Left Ventricle: 3D Flow Past Biological and Mechanical Heart Valves

Article Type: Full Length Article (max 3500 words)

Keywords: Particle image velocimetry, Tomographic PIV, left ventricle flow, prosthetic heart valves

Corresponding Author: Mr. Hicham Saaid,

Corresponding Author's Institution:

First Author: Hicham Saaid

Order of Authors: Hicham Saaid; Jason Voorneveld; Christiaan Schinkel; Jos Westenberg; Frank Gijsen; Patrick Segers; Pascal Verdonck; Nico De Jong; Johan G. Bosch; Sasa Kenjeres; Tom Claessens

Abstract: Left ventricular flow is intrinsically complex, three-dimensional and unsteady. Its features are susceptible to cardiovascular pathology and treatment, in particular to surgical interventions involving the valves (mitral valve replacement). To improve our understanding of intraventricular fluid mechanics and the impact of various types of prosthetic valves thereon, we have developed a custom-designed versatile left ventricular phantom with anatomically realistic moving left ventricular membrane. A biological, a tilting disc and a bileaflet valve (in two different orientations) were mounted in the mitral position and tested under the same settings. To investigate 3D flow within the phantom, a four-view tomographic particle image velocimetry setup has been implemented. The results compare side-by-side the evolution of the 3D flow topology, vortical structures and kinetic energy in the left ventricle domain during the cardiac cycle. Except for the tilting disc valve, all tested prosthetic valves induced a crossed flow path, where the outflow crosses the inflow path, passing under the mitral valve. The biological valve shows a strong jet with a peak velocity about twice as high compared to all mechanical heart valves, which makes it easier to penetrate deeply into the cavity. Accordingly, the peak kinetic energy in the left ventricle in case of the biological valve is about four times higher than the mechanical heart valves. We conclude that the tomographic particle imaging velocimetry setup provides a useful ground truth measurement of flow features and allows a comparison of the effects of different valve types on left ventricular flow patterns.

Cover Letter

To: Dr. Editor-in-chief

Journal of Biomechanics

09 November 2019

Dear Professor,

I am pleased to submit an original article entitled “Tomographic PIV in a Model of the Left Ventricle: 3D Flow Past Biological and Mechanical Heart Valves” by Saaid et al. (corresponding author: hicham.saaid@ugent.be), We hope that this article will be considered for publication to the Journal of Biomechanics.

The following work is part of the project “4Dflow heart”, in which different research groups are involved: Erasmus Medical Centre (EMC), Delft University of Technology (TU Delft), Leiden University Medical Centre (LUMC) and Ghent University. The goal is to develop a versatile and reproducibly hydraulic setup that mimics as closely as possible the flow in a left ventricle model. The developed phantom will be used as a validation platform for emerging medical imaging techniques.

This study, to our best knowledge, is the first to investigate the three-dimensional flow structures within a realistically shaped left ventricle model using a volumetric particle image velocimetry technique (tomographic PIV). In particular, the aims of the present study were: i) demonstrate the feasibility of a tomographic, full-volumetric PIV technique to dynamically capture the 3D flow in a realistic LV model and ii) to compare the flow field generated by three of the most commonly implanted prosthetic heart valves (biological, tilting disc and bileaflet) under the same running conditions

All of the authors were fully involved in the study and have made substantial contributions in varying degrees to the conception, design, experimental setup, acquisition and analysis of data, preparation and review of the manuscript. This manuscript has not been published and is not under consideration for publication elsewhere.

Yours sincerely,

Hicham Saaid

*Revision Notes

Tomographic PIV in a Model of the Left Ventricle:

3D Flow Past Biological and Mechanical Heart Valves

Hicham Saaid[1], Jason Voorneveld[2], Christiaan Schinkel[3], Jos Westenberg[4], Frank Gijsen[2], Patrick Segers[1], Pascal Verdonck[1], Nico de Jong[2] , Johan G. Bosch[2], Sasa Kenjeres[3],Tom Claessens[5]

1 Institute Biomedical Technology, Ghent University, Ghent, Belgium

2 Department of Biomedical Engineering, Thoraxcenter, Erasmus MC University Medical Center, Rotterdam, The Netherlands

3 Department of Chemical Engineering, Faculty of Applied Sciences, Delft University of Technology, Delft, The Netherlands

4 Department of Radiology, Leiden University Medical Center, Leiden, The Netherlands

5 Department of Materials, Textiles and Chemical Engineering, Ghent University, Ghent, Belgium

Ref.: Ms. **No. BM-D-18-01151**

A detailed point-by-point commentary to the comments of all reviewers has been prepared by the authors. The authors presume that these answers address the main concerns of the reviewers and remain available to consider specific suggestions to further improve the reach of the present study.

Legend:

In blue: Reviewer's comments

In black: Author's answers

In red: changes in the manuscript

Reviewer #1:

The authors provide detailed information on the flow feature but does not link it the clinical implications. We recognize the importance of vortex in the left ventricle undergoing the influence of heart valve. We are also unsure whether the left ventricle model are from healthy subject or patient with diseased heart. I assume a normal LV do not need an implantation of prosthetic valve. It will be interesting to investigate how the flow features e.g. Formation of multiple vortex can have biological effects on the left ventricle.
Some comments as shown below

We would like first to thank the reviewer for his/her comments on our work and for providing us with the opportunity to clarify some aspects of the work and improve the quality of the manuscript.

Answers to the above questions are given with the corresponding detailed comments below. In general, we want to clarify that the prime purpose of the developed phantom setup was to use tomographic PIV as a ground truth to verify flow measurements by 3D high-framerate ultrasound and phase contrast MRI. The flow inside the phantom is to a sufficient level similar to physiological flow in the LV and reproducible between cycles, but it is not intended to be anatomically super-realistic. It allows a comparison of flow features between different types of valves. However, the phantom could provide a basis for measurements in patients by MRI or ultrasound.

We have clarified this briefly in the introduction section (last paragraph): *Additionally, this phantom is compatible with 3D ultrasound and MRI imaging, such that 3D flow measurements acquired by these in-vivo medical imaging approaches can be compared to the optical ground truth in the future.*

Abstract

The author should state why it is necessary for studying complex flow behaviour inside the left ventricle rather than state the needs of volumetric measurement. Again, please correlate the flow features to the clinical implications. Please don't use abbreviation in the abstract, like PIV and CT. also state clearly what the 150 subject (healthy or patient) is? The current abstract do not have a conclusion of study, please include it.

1-The abstract section has been adapted based on the reviewer's comments.

The following was added at the beginning of the abstract section: *Left ventricular flow is intrinsically complex, three-dimensional and unsteady. Its features are susceptible to cardiovascular pathology and treatment, in particular to surgical interventions involving the valves (mitral valve replacement). To improve our understanding of intraventricular fluid mechanics and the impact of various types of prosthetic valves thereon, we have developed a custom-designed versatile left ventricular phantom with anatomically realistic moving left ventricular membrane.*

2-The left ventricle shape is based on CT scans of patients with (suspected) cardiac problems. We have pasted a snippet below from the two papers on the CT images (attached):

(Metz et al. 2012)'The scans were made for clinical diagnosis of patients presenting acute or stable chest pain symptoms suspicious for obstructive coronary artery disease or for research purposes and represent large variability in anatomy and pathologies'

(Kirişli et al. 2010) 'These images were acquired for clinical diagnosis and follow-up of patients with (suspected) cardiac problems. Therefore, the images exhibit different types of pathology and also include stents and pacemakers'

Indications regarding the type of subject have been included in the material and methods section: *The shape of the LV mould was extracted from the statistical mean of a dataset of segmented 4D computed tomography images of 150 patients (Kirişli et al. 2010; Metz et al. 2012; Voorneveld et al. 2018).*

3- The following conclusion has been added to the abstract section: *We conclude that the tomographic particle imaging velocimetry setup provides a useful ground truth measurement of flow features and allows a comparison of the effects of different valve types on left ventricular flow patterns.*

2. Introduction

Please include a paragraph how the flow features change the behaviour of left ventricle.

A new paragraph has been included in the introduction section based on the referee's comment: *The left ventricle (LV) is believed to preserve the momentum of the incoming blood flow during diastole by keeping it in motion during diastasis and smoothly redirecting it towards the outflow tract during systole (Kim et al. 1995; Kilner et al. 2000). The topology of these flow structures is determined by the geometry of the LV cavity, the morphology of the mitral valve and the electrical conduction system (Bermejo et al. 2015; Mele et al. 2018). Various multidisciplinary studies have been conducted to better understand the pathophysiology of heart disease, to define clinically useful indicators of cardiac function (Gharib et al. 2006; Belohlavek 2012) and/or to understand the effect of mitral valve repair or replacement by a prosthetic device on the LV flow* (Raghav 2018). *The choice of a biological vs. mechanical prosthesis for instance is still an open debate (Chikwe 2018) as shown in a recent observational study by (Goldstone 2017).*

There is a number of PIV studies focus on the 3D PIV of left ventricle recently. Do include them in the manuscript rather than citing 2D PIV as limitation. You can search them in Journal of experimental fluids or journal of Biomechanics.

As mentioned and cited in the manuscript, we are aware of different works on reconstructing 3D flow in the left ventricle by combining either standard PIV (2C-2D) or stereoscopic PIV (3C-2D) data obtained in a series of parallel or cross-parallel planes. To the best of our knowledge, however, there are no published works about *tomographic* PIV in LV model to obtain an instant measurement of all flow velocity vectors. We have conducted further research, as suggested by the reviewer, in the Journal of Experiments in Fluids and the Journal of Biomechanics, and other reference scientific journal databases with no results. Instead, we would like to cite some works using tomographic PIV for other biomedical flow investigations, such as in the aortic root (Hasler et al. 2016; 2018), the carotid artery (Buchmann et al. 2011) and the intracranial aneurysm (Roloff et al. 2018).

Please find below a list of published works using different PIV modalities within a LV model. Most of these references are in the manuscript. Abbreviations: Two velocity components PIV (2C-2D) – Three velocity components PIV (3C-2D) – right atrium model (RA).

2C- 2D PIV	**3C- 2D PIV**	**Reconstructed 3D flow field** *(from data)*
(Pierrakos et al. 2004)	(Akutsu and Masuda 2003)	(Fortini et al. 2013) (2C-2D)
(Falahatpisheh et al. 2012)	(Guo et al. 2016)	(Falahatpisheh et al. 2014) (2C-2D) *RA*
(Espa et al. 2012)	(Saaid et al. 2018)	(Guo et al. 2016) (3C-2D)
(Vedula et al. 2014) *CFD + 2C-PIV*		(Saaid et al. 2018) (3C-2D) Single calib.
(Vukićević et al. 2012)		
(Okafor et al. 2015)		
(Tan et al. 2016)		
(Fortini et al. 2013)		
(Voorneveld et al. 2017)		

The following was added to the manuscript in the introduction section: *To date, Tomo-PIV has been used for studying the blood flow in the aortic root (Hasler et al. 2016; Hasler and Obrist 2018), the carotid artery (Buchmann et al. 2011) and the intracranial aneurysm (Roloff et al. 2018).*

3. Method

Section 2.1 Please confirm the dataset is from healthy or disease model. Also state if the author has obtained ethics approval to use it.

The left ventricle shape is based on CT images of 150 patients (please see answer in the abstract section). The data were previously acquired and have been used in previously published papers. Therefore, ethical approval specific for this manuscript was not required, but we had of course the approval to reuse the data for our study.

This is now mentioned in the manuscript in the Materials and Methods (Left ventricle membrane and tank undersection): *The shape of the LV mould was extracted from the statistical mean of a dataset of segmented 4D computed tomography images of 150 patients (Kirişli et al. 2010; Metz et al. 2012; Voorneveld et al. 2018).*

The silicon refractive index was measured but the author should state whether it is good enough. Please provide the references on it.

Firstly, we have measured the refractive index of a thin piece of silicone. After that, we have slightly adjusted the fluid mixture (60% glycerol and 40% distilled water) iteratively and measured the refractive index of the fluid to match the refractive index of the silicone. **Qualitatively**, we can check if there is any distortion by placing a calibration plate behind the membrane. **Fig X1** shows that the markers of the target change only in

intensity without distortions. **Quantitatively**, any residual optical distortion after the refractive index matching has been corrected during volume-self calibration (Wieneke 2008). Therefore, we would like to point out that the disparity error (average of 0.02 pixel) after the volume-self calibration was below the recommended value (0.1) from literature (Scarano 2012)

The following was added to the Materials and Methods (Working fluid and tracer particles undersection): *The ratio of the components in the fluid mixture (60% glycerol and 40% distilled water) was adjusted until its measured refractive index (1.4140) very closely matched that of the silicone.*

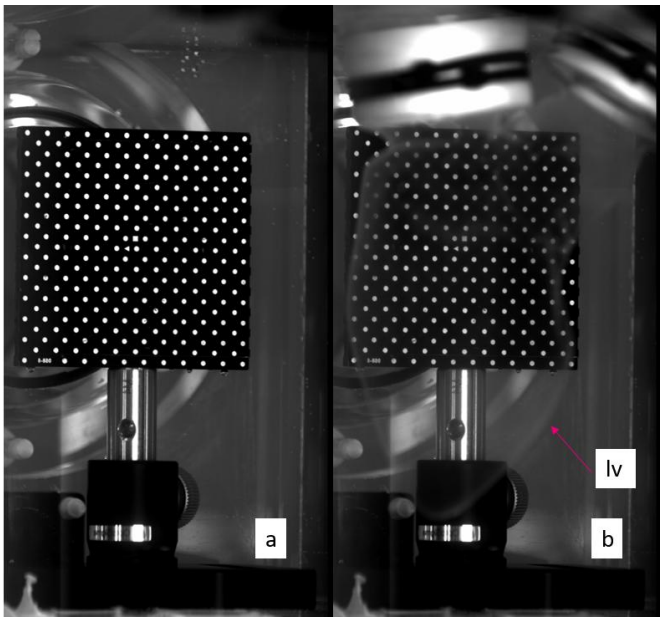

Fig X1 a) calibration plate placed within the tank. b) LV membrane positioned in front of the target.

The thickness of LV membrane should be justified. It is unclear if 0.5 mm is enough to represent left ventricle wall.

A 0.5 mm silicone membrane is not enough to represent the mechanical properties of the whole LV wall, but this is not the prime purpose of our setup. The phantom is designed to be optically transparent for tomographic (and stereoscopic) PIV, and at the same time allow flow imaging by 3D ultrasound and MRI. The purpose is to generate repeatable flow patterns that mimic the dynamics of intraventricular flow in humans, for comparing different imaging modalities. We have to make compromises in the realism of the mechanical behaviour and properties of the ventricle. The membrane only delineates the endocardial border (as in previous LV in vitro studies). In biomedical fluid PIV experiments the models mostly are either rigid or flexible. The first ones are made by silicone casts and are specifically used in vascular experiments. The second type of models are fabricated by deep moulding techniques or by painting the silicone on a mould. Given the large deformations undergone by the LV endocardial shape for supplying the pumping function of the ventricle, the latter technique has been used in the present work.

We have added an explanation in the introduction section (last paragraph), to clarify this: *Additionally, this phantom is compatible with 3D ultrasound and MRI imaging, such that 3D flow measurements acquired by these in-vivo medical imaging approaches can be compared to the optical ground truth in the future.*

We also added in the Materials and Methods (caption figure 1): (a) *3D-printed LV mould representing the endocardial shape at end systole, fitted with a mitral inflow and aortic outflow tract.*

Variable resistance is unclear, please rephrase it.

The outlet from the aortic chamber is connected to the atrial chamber via a peripheral resistance controller (Vivitro Labs Inc., Canada) with a short length of silicone rubber hose. The peripheral resistance can be adjusted with a rotational control which affects the aortic pressure.
The following was added in the Materials and Methods (Left ventricle membrane and tank undersection): *The outlet from the aortic chamber is connected to the left atrial chamber via an adjustable peripheral resistance valve (Vivitro Labs Inc., Victoria, BC, Canada) with a short length of silicone rubber hose.*

Suggest write BPM in full words before using it as abbreviation. Has been changed to beats per minute

Section 2.7

The author should state how many images are taken and also whether a convergence analysis for the tomographic PIV is conducted and also the relative error for number of images.

In order to perform the Tomo-PIV measurements in a phase-locked manner, the PIV system was triggered with the pulsatile pump. However, due to some technical limitations (LaVision acquisition software), we had to acquire the full cardiac cycle (1714 time points) instead of acquiring only selected time points for each cardiac cycle (phase-locked manner).

We have acquired data from 30 cardiac cycles (only in case of the biological valve), the sampling rate was 2 kHz for a cardiac cycle of 857 ms (70 BPM) which corresponds to 1714 images per cycle. In the present work, we present the data of a subset of 61 equidistant time points, phase averaged from ten cycles. We have performed only a semi-qualitative convergence analysis and compared the results of phase averaged data obtained from 10, 20 and 30 cycles. Figure X2 compares the evolution of the velocity magnitude averaged in the black rectangle in the three ensemble data sets. The box is centred in the region of the high velocity jet past the biological valve. This simple test shows that the ensemble of ten cardiac cycles finds slightly higher velocity than the average of 20 or 30 cycles. Considering that the present work is a comparative study and in order to limit the processing time, we have opted to average ten cardiac cycles.

The following has been added to the limitation section: *Due to computational cost and amount of data storage, we have presented only the averaged flow field data based on 10 cycles. A semi-quantitative convergence analysis (consisting of a comparison between the phase averaged data obtained from 10, 20 and 30 cycles) showed no discernible difference between 20 and 30 cycles. Only at peak early inflow a 7% difference in flow velocity was found between the results obtained with 10 cycles and the converged flow velocity data using 30 cycles.*

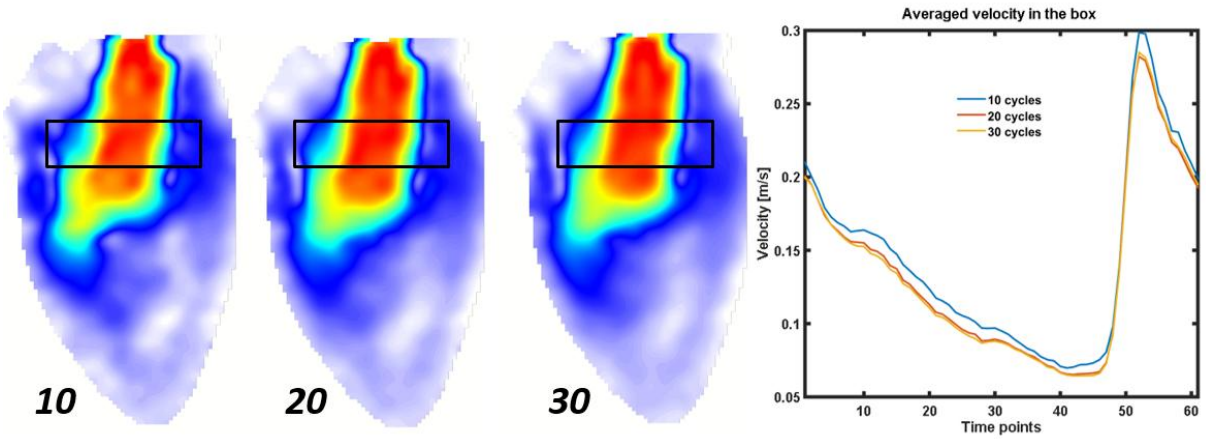

Fig X2: *Left:* cross-section of velocity vector field averaging 10, 20 and 30 cardiac cycles. *Right:* Comparison of the temporal evolution of the averaged velocity calculated in the black box

Note also that each data set of ten cycles was approximately 200 Gigabytes (only raw data) without considering pre / and post-processing. Consequently, acquiring 20 cycles for four valve types would mean adding one

terabyte of data. A second factor is the required processing time (calculation of the 3D velocity vector field starting from the raw PIV images). The tomographic PIV software needs approximately 10 min per time instant.

Results and discussion

Fig. 2 suggest state the meaning of **W** and also give caption to vertical axis. Replace the yellow colour arrow with red colour and make it more visible.

The figure and caption have been changed as suggested.

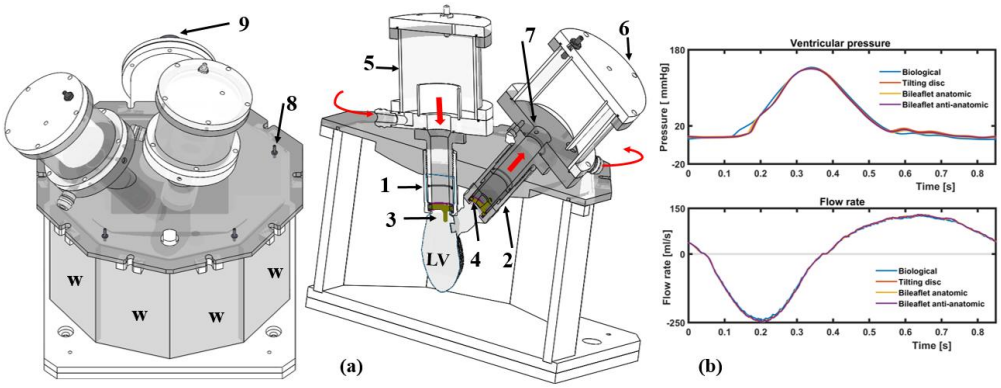

***Caption* Fig. 2.** *(a) CAD view of the nine-sided tank. The shape of the tank provides undistorted optical access to the LV from different angles. W indicates the four windows used for optical access. The red arrows depict the LV flow loop.*

Fig.4 (b) please state what is vertical axis and also for subsequent graph:
The figure has been changed as suggested

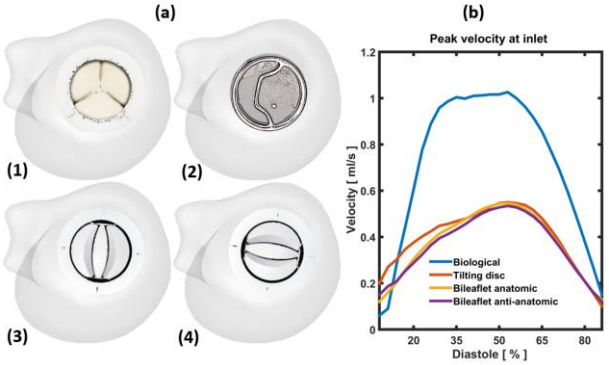

Figure 8, please overlap the both figure to see the differences of biological and prosthetic valve. The shape of kinetic energy of BHV are quite difference from the MHV. Suggest the author quantify the difference in terms of percentage.

The figure has been changed as suggested.
We would like to point out that during the revision of the paper we have noticed that the values of the kinetic energy were wrong. We have recalculated the KE based on the same formula mentioned in the paper. The range of maximum kinetic energy values in the left ventricle (in mJ) now corresponds to earlier works like (Hussaini et al. 2015).

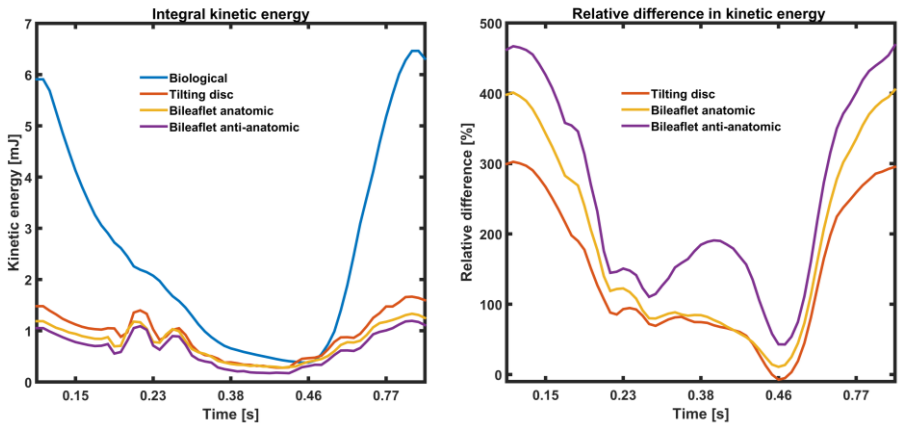

Fig. 8. Left: the evolution of the kinetic energy within the LV domain, computed over the cardiac cycle as: $KE = 0.5\rho \int V^2 dv$, where $\rho = 1060\, kg/m^3$ and V is velocity magnitude. Right: The difference of KE in the biological valve relative to each of the mechanical valves, calculated as: $100\% * (\mathrm{BHV} - \mathrm{MHV_i})/\mathrm{MHV_i}$

Again please correlate the findings to clinical implication.

We have provided some clinical implications in the Results & discussion and Conclusion sections

In the Results and discussion (Inflow characteristics undersection): *Compared to the MHVs, the inflow jet through the BHV is more likely to reach and wash out the apical region. This potentially avoids stagnation zones and reduces the risk for thrombosis formation. In patients with dilated cardiomyopathy or myocardial infarction, where abnormal flow patterns are known to promote blood stasis between the apex and outflow tract (Dantzig 1995; Sengupta et al. 2008; Hendabadi et al. 2013), we would expect the BHV to perform better than the MHVs.*

In the Conclusions section: *Finally, we showed that the anatomic orientation of the bileaflet valve yields an overall slightly higher kinetic energy than the anti-anatomic configuration. Yet, none of our performed analyses reveal that one orientation of the bileaflet valve is to be preferred over the other*.

e.g. Line 262 KE is higher than BHV compared to MHV so does it means MHV will not perform as good as BHV?

Based only on the kinetic energy plot we can tell how much and for how long this energy is present. Indeed, the biological valve yields higher KE than the mechanical valves, with a more than fourfold difference during diastole. However, in case of the biological valve this energy is dissipated more rapidly compared to the MHVs. The energetic parameters (also Lagrangian analysis) of the flow dynamic are subject for further investigations.

Line 224: Showing the jet entering the LV cavity stagnates more closely to the apex, so will it cause platelet aggregation?

The inflow jet from the biological valve impacts (collides) on the anterior wall closer to the LV apex compared to the bileaflet valve, so there is less chance of blood stagnation in the apex. The capability of the blood stream in reaching the apex has been shown in figure 6. However, this latter does not provide a measure of the blood stasis (residual volume). Regarding the platelet aggregation, it has been shown that myocardial infarction can lead to an abnormal flow pattern that causes blood stasis between the apex and outflow tract increasing thrombosis formation (Dantzig 1995; Sengupta et al. 2008; Hendabadi et al. 2013).

We have explained this further in the Results and discussion (Inflow characteristics undersection**:** *The stagnation phenomena in a LV have also been reported in a 2D-PIV investigation by Faludi and co-workers (Faludi et al. 2010), showing that the jet entering the LV cavity collides more closely to the apex with a biological valve than*

with a bileaflet valve. Compared to the MHVs, the inflow jet through the BHV is more likely to reach and wash out the apical region. This potentially avoids stagnation zones and reduces the risk for thrombosis formation. In patients with dilated cardiomyopathy or myocardial infarction, where abnormal flow patterns are known to promote blood stasis between the apex and outflow tract (Dantzig 1995; Sengupta et al. 2008; Hendabadi et al. 2013), we would expect the BHV to perform better than the MHVs.

Suggest the author list E/A ratio as part of limitation if it is not included in current study. If they can be incorporate in the results and discussion it will be better.

We have mentioned this shortcoming and its effects on the LV flow dynamics in more details in the limitations section**:**

Furthermore, the piston pump was driven by a sinusoidal-like wave form that does not represent diastasis and the late filling (A-wave). Consequently, it was not possible to investigate the interaction between the flow structures induced at the early filling and the fresh fluid entering during the late filling wave, as described in vivo (Elbaz et al. 2014) and in a recent numerical simulation study (Khalafvand et al. 2018), using a similar LV geometry and a more realistic flow waveform.

Conclusion

The conclusion should be rewritten. The present work does not state the clinical implication of valve to the ventricle. Furthermore, applying tomographic PIV on studying the flow features in left ventricle is not new. The experimental setup is nice, but the authors should stick to the fact.

Some potential clinical implications have been added in Results and discussion and conclusion section. For the tomographic PIV, as mentioned earlier, we have searched existing academic databases and in particular J. Exp. fluids and J Biomech.) for ‘tomographic PIV left ventricle’, ‘tomographic particle image velocimetry left ventricle’ and the same with ‘ventricle’ and ‘heart’. We could not find any tomographic PIV studies performed in the left ventricle. If the reviewer could kindly provide these references, we would be glad to include them and adjust our conclusions appropriately.

Minor comments

Line 156: "a25mm" should change to a "25mm". Has been corrected

Reviewer #2:

This paper deals with experimental modelling of flow dynamics within deformable left ventricle (LV). The authors group has been working on this subject for a long time.
Two goals are investigated:
i) demonstrate the feasibility of tomographic full volumetric PIV measurements to describe the flow dynamics in a LV model;
ii) Compare the flow behaviour generated by 3 types of mitral valvular prosthesis.

Main questionings

In one of the last paper of the authors group on the subject ([1] Saaid H, Segers P, Novara M, et al (2018) Exp Fluids 59:1-13) the authors proposed to present the capability of scanning stereo-PIV measurements to investigate the full 3D dynamics within the LV. They concluded on the efficiency of this PIV set up, with relatively low end hardware and software when compared to tomographic PIV, to reconstruct the 3D flow patterns in a deformable LV. They also highlighted that this set up needed only one single calibration to determine 3D flow.
So, the reviewer wonders about the implementation of tomographic PIV in the present paper. Why do the authors now think that tomography PIV is essential to reconstruct the 3D flow field and why do they mention in the introduction of the present paper that scanning stereo-PIV set-up of Saaid's paper ([1]) requires complex setups and time consuming calibration procedures?

Both setups present advantages and disadvantages and we would like to answer the following questions by showing the differences between the previous [1] and the present setup [2] in terms of

(i) components and composition
(ii) calibration
(iii) acquisition and processing time

[1] Single calibration multiplane stereoscopic PIV (MSPIV)
[2] Tomographic PIV (Tomo-PIV)

- In terms of PIV apparatus components (e.g. number of cameras and software), the MSPIV setup consists of relatively low-end hardware and software with respect to the Tomo-PIV. However, in the present work we have implemented four-view Tomo-PIV using two cameras with a mirror system. Additionally, the previous setup required two Plexiglas tanks to keep the magnification factor constant throughout the scanning space. The Tomo-PIV setup needed only one tank instead, with a more complex geometry, providing multiple optical access faces for the tomographic cameras.

- In the MSPIV, the physical calibration was performed only in the center plane. However, in order to guarantee the same mapping function throughout the scanning volume, special care has been taken to ensure optimal mechanical alignment of the slide rail on which the stereo-PIV components have been mounted. Conversely, the Tomo-PIV does not require physical alignment between illumination and calibration target. However, Tomo-PIV needed physical calibration at different position in the volume of interest. Additionally, Tomo-PIV is sensitivity to vibrations which may lead to camera misalignment during measurements. To overcome this, we followed a well assessed procedure for physical calibration followed by the correction of the camera's mapping functions performed with the aid of particle images (volume-self calibration). This latter has been conducted at the beginning and at the end of the measurements to ensure that calibration is maintained throughout the whole sequence of measurements.

- Under the same conditions of temporal resolution and volume of interest, the acquisition time is drastically lower in the case of Tomo-PIV. While in the following work we have presented only phased locked data, we have acquired 1714 time points for each cardiac cycle of the duration of $857ms$. The total acquisition time required was the duration of one cardiac cycle, plus 8 minutes for transferring the

data from the camera to the workstation. Conversely, in the previous work, we have adopted a low-speed camera (15 Hz), where the acquisition procedure consists of recording one time point per 30 cardiac cycles (phase-locked) at each position. After this, the PIV setup has to be translated to the next position and the procedure must be repeated in order to cover the region of interest.

Conclusion: Considering the above, both setups have their pros and cons. The MSPIV is more similar to traditional multiplane setups and has some advantages (apparatus costs, sensitivity to vibrations and laser sheet-calibration target alignment) over tomographic PIV. The latter is significantly more expensive in terms of components and software, but is more practical for setup and for time resolved acquisition. Therefore, the scope of the present work was to illustrate the feasibility of the tomographic PIV technique in a transparent and dynamic model and to compare prosthetic valves under similar conditions.

We have explained this further in the Limitations section: *Despite the aforementioned advantages of the employed technique, some limitations are worthwhile mentioning. Tomo-PIV hardware and software are generally more complex and expensive than 2D PIV or multiplane scanning setups. However, to reduce the cost of the PIV apparatus, a four-view Tomo-PIV imaging system has been implemented using a combination of only two cameras (instead of four) and a mirror system. Also, while Tomo-PIV does not require physical alignment between illumination and the calibration target, it is more sensitive to vibrations compared to stereoscopic PIV, which may lead to camera misalignment during the acquisition. To overcome this, we followed a well-established procedure for physical calibration, followed by the volume-self calibration.*

In the present work, the authors investigated the flow field generated in the LV by a 25mm bileaflet mitral valve (Sorin biomedica) which was mounted in two different orientations (anatomic and anti-anatomic) while a 19mm tricuspid valve was used as aortic valve. Lambda 2 method has been used to identify 3D flow characteristics; TKE is computed.
The paper in experiment in fluids ([1]) described the effects of the orientation 25mm bileaflet mitral valve (Carbomedics) while a 19mm bileaflet valve was used as aortic valve. Lambda 2 method has been used to identify 3D flow characteristics; TKE is computed.
It is therefore worth noticing that aortic valvular prosthesis were different and the geometry of the deformable LV also. However, it would be of first importance that the authors present the main differences as far as the obtained 3D flow is concerned. Is the new configuration, tricuspid aortic valve prosthesis and more anatomic LV geometry, highlights an important point?

In the previous work the LV has an axisymmetric shape and the LV base diameter was approximately 1.5 times larger than a normal LV. This leads to a different flow path compared to the present work. In the present work, the bileaflet valve, in both orientations, gives rise to a crossed flow pattern with counter-clockwise rotation. Conversely, in the previous work, the inflow jet slides along the posterior wall with clockwise rotation (i.e. the outflow path did not cross the inflow during the ejection phase). We do expect that the aortic valve has far less influence on the intraventricular flow, unless there is a regurgitation flow which interacts and alters the LV flow (Labbio and Kadem 2018). We consider that the anatomical shape of the LV model is a major determinant of intraventricular flow.

A list of the relevant differences between the two setups.

	Previous work	**Present work**
LV shape	Axisymmetric	Statistical shape (more realistic)
Inflow-outflow tracts	Not separated	Separated
Ratio LV diameter / valve	≅ 2.8	≅ 1.8
Filling	E and A wave	pseudo-sinusoidal (no A wave)
Density [kg/m^3]	1750	1160
Dynamic viscosity [mPa s]	5.77	17.7

We have provided some indications of the differences between the two studies in the Results and discussion (Flow velocity field undersection): *Additionally, our results indicate that in both configurations the bileaflet valve gives rise to a crossed flow path. This confirms the findings from a prior in vivo study from (Faludi et al. 2010). Conversely,* (Nakashima et al. 2017)*, using an ultrasound based vector flow mapping technique, showed that only the anti-anatomical orientation is associated with a crossed flow path. In our previous work (Saaid et al. 2018), we even observed that both orientations lead to a looped flow path. Some of the discrepancies may be due to the highly simplified LV shape and the different LV diameter/valve ratio (Saaid et al. 2018) or a limitation of two-dimensional echocardiography in case of (Nakashima et al. 2017).*

The authors present different combinations associating mitral and aortic valvular prostheses. Can the authors explain what motivated their associated valve pair choice? Is tilting disc valve still often implanted? Can the authors link the flow behaviour in LV with the use of a specific valve pair which would be optimal for the patients? with **the surgeon's questionings**? with particular clinical events?

The choice of heart valve replacement is still an open debate, especially between biological and mechanical bileaflet valves (Chikwe 2018). The approach of selection is often determined by balancing the risks of anticoagulation and reoperation. In a recent article published by Goldstone et al. (2017), an observational study, the results indicate that the use of biological valves was associated with a higher risk of reoperation than the use of mechanical valves (Goldstone et al. 2017). These findings were associated with increased structural valve degeneration and not with alterations in flow dynamics. In young patients, mitral valve repair is preferred when it is possible (does not expose the patient to an unacceptable risk of reoperation). Mitral valve repair does not only preserve anatomical elements but also maintains the physiological intraventricular flow dynamics and is energetically more efficient compared to valve replacement (Akiyama et al. 2017).

We agree with the reviewer's concern that the tilting disc valve has an old design and is almost not implanted anymore in the Western world. However, we believe it was worthwhile to compare tilting disc valve with the most commonly implanted heart valves, as quite a lot of experimental and numerical data on hemodynamic performance of the tilting disk valve is available (e.g. Akutsu 1999; Kaminsky et al. 2007; Querzoli et al. 2010; Vukićević et al. 2012).

The following has been added to the manuscript, introduction section (second paragraph): *Various multidisciplinary studies have been conducted to better understand the pathophysiology of heart disease, to define clinically useful indicators of cardiac function (Gharib et al. 2006; Belohlavek 2012) and/or to understand the effect of mitral valve repair or replacement by a prosthetic device on the LV flow (Raghav 2018). The choice of a biological vs. mechanical prosthesis for instance is still an open debate (Chikwe 2018) as shown in a recent observational study by (Goldstone 2017).*

We have explained this further in the Results and discussion (Inflow characteristics undersection**:** *Compared to the MHVs, the inflow jet through the BHV is more likely to reach and wash out the apical region. This potentially avoids stagnation zones and reduces the risk for thrombosis formation. In patients with dilated cardiomyopathy or myocardial infarction, where abnormal flow patterns are known to promote blood stasis between the apex and outflow tract (Dantzig 1995; Sengupta et al. 2008; Hendabadi et al. 2013), we would expect the BHV to perform better than the MHVs.*

Other points:

Physiological flow rate and pressures could be added on figure 2b to appreciate the similarity / discrepancy with the experimental ones.

We agree that it is quite common to include information about physiological flow curves. However, we have mentioned the differences between the physiological and the imposed hydraulic settings in the limitation section. To avoid any confusion, we opted to only show the measured flow data.

The following was added to the limitation section*: Furthermore, the piston pump was driven by a sinusoidal-like wave form that does not represent diastasis and the late filling (A-wave). Consequently, it was not possible to*

investigate the interaction between the flow structures induced at the early filling and the fresh fluid entering during the late filling wave, as described in vivo (Elbaz et al. 2014) and in a recent numerical simulation study (Khalafvand et al. 2018), using a similar LV geometry and a more realistic flow waveform.

The dynamic viscosity of the working fluid seems very high compared to blood one -17.7 mPas versus 3-4 mPas respectively. Why this choice? What is the influence of this value on the flow behaviour? What is its refractive index value?

We agree with the reviewer on the fact that the fluid adopted in the present work is much more viscous than blood. A higher value of dynamic viscosity may have effects on the flow resistance and consequently on viscous dissipation of the vortical structures and may contribute to or attenuate this flow organization.
In order to avoid any distortion, we have opted to use a fluid mixture that "perfectly" matches the refractive index of the silicone membrane. The refractive index of the fluid mixture is 1.4130, measured at 22 °C. Additionally, the used fluid solution permits testing biological material. In the previous work we have adopted a fluid mixture (sodium iodide, glycerol and distilled water) with dynamic viscosity of 5.7 mPa. However, one of the disadvantages of sodium iodide mixture is that is not possible to test biological valves (dehydration of the leaflets).

Added to the manuscript, limitations section: *Also, the working fluid mixture has a dynamic viscosity four times higher than blood, which may have affected the flow resistance and consequently the formation and viscous dissipation rate of the vortical structures.*

Ten consecutive cardiac cycles were averaged for each heart valve configuration. Why this value?
Did the authors obtain a good statistical convergence with this value?

In order to perform the Tomo-PIV measurements in a phase-locked manner, the PIV system was triggered with the pulsatile pump. However, due to some technical limitations (LaVision acquisition software), we had to acquire the full cardiac cycle (1714 time points) instead of acquiring only selected time points for each cardiac cycle (phase-locked manner).

We have acquired data from 30 cardiac cycles (only in case of the biological valve), the sampling rate was 2 kHz for a cardiac cycle of 857 ms (70 BPM) which corresponds to 1714 images per cycle. In the present work, we present the data of a subset of 61 equidistant time points, phase averaged from ten cycles. We have performed only a semi-quantitative convergence analysis and compared the results of phase averaged data obtained from 10, 20 and 30 cycles. Figure X3 compares the evolution of the velocity magnitude averaged in the black rectangle in the three ensemble data sets. The box is centred in the region of the high velocity jet past the biological valve. This simple test shows that the ensemble of ten cardiac cycles finds slightly higher velocity than the average of 20 or 30 cycles. Considering that the present work is a comparative study and in order to limit the processing time, we have opted to average ten cardiac cycles.

The following has been added to the limitation section: *Due to computational cost and amount of data storage, we have presented only the averaged flow field data based on 10 cycles. A semi-quantitative convergence analysis (consisting of a comparison between the phase averaged data obtained from 10, 20 and 30 cycles) showed no discernible difference between 20 and 30 cycles. Only at peak early inflow a 7% difference in flow velocity was found between the results obtained with 10 cycles and the converged flow velocity data using 30*

cycles.

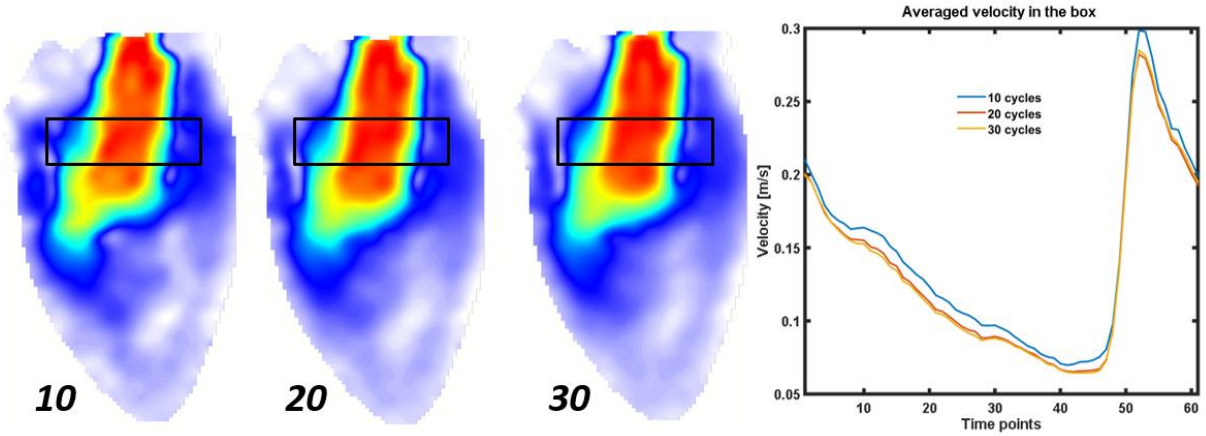

Fig X3: *Left:* cross-section of velocity vector field averaging 10, 20 and 30 cardiac cycles. *Right:* Comparison of the temporal evolution of the averaged velocity calculated in the black box

Note also that each data set of ten cycles was approximately 200 Gigabytes (only raw data) without considering pre / and post-processing. Consequently, acquiring 20 cycles for four valve types would mean adding one terabyte of data. A second factor is the required processing time (calculation of the 3D velocity vector field starting from the raw PIV images). The tomographic PIV software needs approximately 10 min per time instant.

Can the authors put into light what it is new in the velocity flow field description compared to the literature quoted in the 3.1 paragraph.

We have changed the paragraph according to the reviewer's comments.

In the anti-anatomic orientation (Fig 5d), on the other hand, the flow pattern through the outer orifices appears to be nearly symmetric (time steps II-III). In both configurations, at mid diastole the strong central jet merges with the outer jets towards the apex. The iso-velocity surface emanating from the mitral valve dissipates before reaching the apex (Fig 5c-d), as previously described in (Pierrakos et al. 2004). *Additionally, our results indicate that in both configurations the bileaflet valve gives rise to a crossed flow path. This confirms the findings from a prior in vivo study from (Faludi et al. 2010). Conversely,* (Nakashima et al. 2017)*, using an ultrasound based vector flow mapping technique, showed that only the anti-anatomical orientation is associated with a crossed flow path. In our previous work (Saaid et al. 2018), we even observed that both orientations lead to a looped flow path. Some of the discrepancies may be due to the highly simplified LV shape and the different LV diameter/valve ratio (Saaid et al. 2018) or a limitation of two-dimensional echocardiography in case of (Nakashima et al. 2017).*

References

Akiyama K, Nakamura N, Itatani K, et al (2017) Flow-dynamics assessment of mitral-valve surgery by intraoperative vector flow mapping. 24:869–875. doi: 10.1093/icvts/ivx033

Akutsu T (1999) Effect of mechanical prosthetic heart valve orientation on the flow field inside the simulated ventricle: comparison between St. Jude Medical Valve and Medtronic-Hall Valve. 39–45.

Akutsu T, Masuda T (2003) Three-dimensional flow analysis of a mechanical bileaflet mitral prosthesis. J Artif Organs 6:112–23. doi: 10.1007/s10047-003-0214-z

Belohlavek M (2012) Vortex formation time: An emerging echocardiographic index of left ventricular filling efficiency? Eur Heart J Cardiovasc Imaging 13:367–369. doi: 10.1093/ejechocard/jer311

Bermejo J, Martínez-Legazpi P, del Álamo JC (2015) The Clinical Assessment of Intraventricular Flows. Annu Rev Fluid Mech 47:315–342. doi: 10.1146/annurev-fluid-010814-014728

Buchmann NA, Atkinson C, Jeremy MC, Soria J (2011) Tomographic particle image velocimetry investigation of the flow in a modeled human carotid artery bifurcation. Exp Fluids 50:1131–1151. doi: 10.1007/s00348-011-1042-1

Carlhäll CJ, Bolger A (2010) Passing strange flow in the failing ventricle. Circ Hear Fail 3:326–331. doi: 10.1161/CIRCHEARTFAILURE.109.911867

Chennakeshavallu GN, Gadhinglajkar S, Sreedhar R, Bhaskar PP PV (2017) Anatomical vs Anti-anatomical Placement of a Tilting-disk Mechanical Valve in Mitral Position. J Perioper Echocardiogr 2017 5(1):12–15.

Chikwe (2018) Prosthesis Type for Aortic- and Mitral-Valve Replacement. 776–779. doi: 10.1056/NEJMc1715189

Dantzig JM Van (1995) Doppler Left Ventricular Flow Pattern Versus Conventional Predictors of Left Ventricular Thrombus After Acute Myocardial Infarction. 25:1341–1346. doi: 10.1016/0735-1097(94)00548-5

Elbaz MSM, Calkoen EE, Westenberg JJM, et al (2014) Vortex flow during early and late left ventricular filling in normal subjects: quantitative characterization using retrospectively-gated 4D flow cardiovascular magnetic resonance and three-dimensional vortex core analysis. J Cardiovasc Magn Reson 16:78. doi: 10.1186/s12968-014-0078-9

Espa S, Badas MG, Fortini S, et al (2012) A Lagrangian investigation of the flow inside the left ventricle. Eur J Mech B/Fluids 35:9–19. doi: 10.1016/j.euromechflu.2012.01.015

Falahatpisheh A, Kheradvar A (2012) High-speed particle image velocimetry to assess cardiac fluid dynamics in vitro: From performance to validation. Eur J Mech B/Fluids 35:2–8. doi: 10.1016/j.euromechflu.2012.01.019

Falahatpisheh A, Pedrizzetti G, Kheradvar A (2014) Three-dimensional reconstruction of cardiac flows based on multi-planar velocity fields. Exp Fluids. doi: 10.1007/s00348-014-1848-8

Faludi R, Szulik M, D'hooge J, et al (2010) Left ventricular flow patterns in healthy subjects and patients with prosthetic mitral valves: An in vivo study using echocardiographic particle image velocimetry. J Thorac Cardiovasc Surg 139:1501–1510. doi: 10.1016/j.jtcvs.2009.07.060

Fortini S, Querzoli G, Espa S, Cenedese a. (2013) Three-dimensional structure of the flow inside the left ventricle of the human heart. Exp Fluids. doi: 10.1007/s00348-013-1609-0

Gharib M, Rambod E, Kheradvar A, et al (2006) Optimal vortex formation as an index of cardiac health. Proc Natl Acad Sci U S A 103:6305–6308. doi: 10.1073/pnas.0600520103

Goldstone (2017) Mechanical or Biologic Prostheses for Aortic-Valve and Mitral-Valve Replacement. 1847–1857. doi: 10.1056/NEJMoa1613792

Guo S, Tan D, Kim S, Liang H (2016) A biomimetic bi - leaflet mitral prosthesis with enhanced physiological left ventricular swirl restorative capability. Exp Fluids 57:1–12. doi: 10.1007/s00348-016-2195-8

Hasler D, Landolt A, Obrist D (2016) Tomographic PIV behind a prosthetic heart valve. Exp Fluids 57:1–13. doi: 10.1007/s00348-016-2158-0

Hasler D, Obrist D (2018) Three-dimensional flow structures past a bio- prosthetic valve in an in-vitro model of the aortic root.

Hendabadi SAH, Ermejo JAB, Enito YOB, et al (2013) Topology of Blood Transport in the Human Left Ventricle by Novel Processing of Doppler Echocardiography. 41:2603–2616. doi: 10.1007/s10439-013-0853-z

Hussaini SF, Roldán-Alzate A, Francois CJ (2015) Left and right ventricular kinetic energy using time-resolved versus time-average ventricular volumes. J Cardiovasc Magn Reson 17:1–8. doi: 10.1002/jmri.25416

Kaminsky R, Kallweit S, Weber HJ, et al (2007) Flow visualization through two types of aortic prosthetic heart

valves using stereoscopic high-speed particle image velocimetry. Artif Organs 31:869–879. doi: 10.1111/j.1525-1594.2007.00471.x

Khalafvand SS, Voorneveld JD, Muralidharan A, et al (2018) Assessment of human left ventricle flow using statistical shape modelling and computational fluid dynamics. J Biomech 74:116–125. doi: 10.1016/j.jbiomech.2018.04.030

Kilner PJ, Yang G, Wilkes AJ, et al (2000) Asymmetric redirection of flow through the heart. 759–761.

Kim WY, Walker PG, Pedersen EM, et al (1995) Left ventricular blood flow patterns in normal subjects: A quantitative analysis by three-dimensional magnetic resonance velocity mapping. J Am Coll Cardiol 26:224–238. doi: 10.1016/0735-1097(95)00141-L

Kirişli HA, Schaap M, Klein S (2010) Evaluation of a multi-atlas based method for segmentation of cardiac CTA data : a large-scale , multicenter , and multivendor study. Am Assoc Phys Med 6279–6291. doi: 10.1118/1.3512795

Labbio G Di, Kadem L (2018) Jet collisions and vortex reversal in the human left ventricle. J Biomech 1–6. doi: 10.1016/j.jbiomech.2018.07.023

Mele D, Smarrazzo V, Pedrizzetti G, et al (2018) Intracardiac Flow Analysis : Techniques and Potential Clinical Applications. J Am Soc Echocardiogr. doi: 10.1016/j.echo.2018.10.018

Metz CT, Baka N, Kirisli H, et al (2012) Regression-Based Cardiac Motion Prediction. 31:1311–1325.

Mittal R, Seo JH, Vedula V, et al (2016) Computational modeling of cardiac hemodynamics: Current status and future outlook. J Comput Phys 305:1065–1082. doi: 10.1016/j.jcp.2015.11.022

Muñoz DR, Markl M, Mur JLM, et al (2013) Intracardiac flow visualization: Current status and future directions. Eur. Heart J. Cardiovasc. Imaging 14:1029–1038.

Nakashima K, Itatani K, Kitamura T, Oka N (2017) Energy dynamics of the intraventricular vortex after mitral valve surgery. Heart Vessels 0:0. doi: 10.1007/s00380-017-0967-6

Okafor I, Santhanakrishnan A, Raghav V, Yoganathan AP (2015) Role of Mitral Annulus Diastolic Geometry on Intraventricular Filling Dynamics. J Biomech Eng 137:1–9. doi: 10.1115/1.4031838

Pedrizzetti GIP, Omenichini FED, Onti GIT (2010) On the Left Ventricular Vortex Reversal after Mitral Valve Replacement. 38:769–773. doi: 10.1007/s10439-010-9928-2

Pierrakos O, Vlachos PP, Telionis DP (2004) Time-resolved DPIV analysis of vortex dynamics in a left ventricular model through bileaflet mechanical and porcine heart valve prostheses. J Biomech Eng 126:714–726. doi: 10.1115/1.1824124

Querzoli G, Fortini S, Cenedese A (2010) Effect of the prosthetic mitral valve on vortex dynamics and turbulence. 1–10. doi: 10.1063/1.3371720

Raghav V (2018) Experimental Assessment of Flow Fields Associated with Heart Valve Prostheses Using Particle Image Velocimetry (PIV): Recommendations for Best Practices. 9:273–287. doi: 10.1007/s13239-018-0348-z

Roloff C, Stucht D, Beuing O, Berg P (2018) Comparison of intracranial aneurysm flow quantification techniques : standard PIV vs stereoscopic PIV vs tomographic PIV vs phase- contrast MRI vs CFD. 1–8. doi: 10.1136/neurintsurg-2018-013921

Saaid H, Segers P, Novara M, et al (2018) Single calibration multiplane stereo-PIV : the effect of mitral valve orientation on three-dimensional flow in a left ventricle model. Exp Fluids 59:1–13. doi: 10.1007/s00348-018-2504-5

Scarano F (2012) Tomographic PIV: principles and practice. Meas Sci Technol 24:012001. doi: 10.1088/0957-0233/24/1/012001

Sengupta PP, Burke R, Khandheria BK, Belohlavek M (2008) Following the Flow in Chambers. 4:325–332. doi: 10.1016/j.hfc.2008.02.005

Tan SG-D, Kim S, Hon JKF, Leo HL (2016) A D-Shaped Bileaflet Bioprosthesis which Replicates Physiological

Left Ventricular Flow Patterns. PLoS One 11:e0156580. doi: 10.1371/journal.pone.0156580

Vedula V, Fortini S, Seo JH, et al (2014) Computational modeling and validation of intraventricular flow in a simple model of the left ventricle. Theor Comput Fluid Dyn 28:589–604. doi: 10.1007/s00162-014-0335-4

Voorneveld J, Member GS, Muralidharan A, et al (2017) High Frame Rate Ultrasound Particle Image Velocimetry for Estimating High Velocity Flow Patterns in the Left Ventricle. IEEE Trans Ultrason Ferroelectr Freq Control PP:1. doi: 10.1109/TUFFC.2017.2786340

Vukićević M, Fortini S, Querzoli G, et al (2012) Experimental study of an asymmetric heart valve prototype. Eur J Mech B/Fluids 35:54–60. doi: 10.1016/j.euromechflu.2012.01.014

Wieneke B (2008) Volume self-calibration for 3D particle image velocimetry. 549–556. doi: 10.1007/s00348-008-0521-5

Tomographic PIV in a Model of the Left Ventricle: 3D Flow Past Biological and Mechanical Heart Valves

Hicham Saaid[1], Jason Voorneveld[2], Christiaan Schinkel[3], Jos Westenberg[4], Frank Gijsen[2], Patrick Segers[1], Pascal Verdonck[1], Nico de Jong[2], Johan G. Bosch[2], Sasa Kenjeres[3], Tom Claessens[5]

1 Institute Biomedical Technology, Ghent University, Ghent, Belgium

2 Department of Biomedical Engineering, Thoraxcenter, Erasmus MC University Medical Center, Rotterdam, The Netherlands

3 Department of Chemical Engineering, Faculty of Applied Sciences, Delft University of Technology, Delft, The Netherlands

4 Department of Radiology, Leiden University Medical Center, Leiden, The Netherlands

5 Department of Materials, Textiles and Chemical Engineering, Ghent University, Ghent, Belgium

Abstract

Left ventricular flow is intrinsically complex, three-dimensional and unsteady. Its features are susceptible to cardiovascular pathology and treatment, in particular to surgical interventions involving the valves (mitral valve replacement). To improve our understanding of intraventricular fluid mechanics and the impact of various types of prosthetic valves thereon, we have developed a custom-designed versatile left ventricular phantom with anatomically realistic moving left ventricular membrane. A biological, a tilting disc and a bileaflet valve (in two different orientations) were mounted in the mitral position and tested under the same settings. To investigate 3D flow within the phantom, a four-view tomographic particle image velocimetry setup has been implemented. The results compare side-by-side the evolution of the 3D flow topology, vortical structures and kinetic energy in the left ventricle domain during the cardiac cycle. Except for the tilting disc valve, all tested prosthetic valves induced a crossed flow path, where the outflow crosses the inflow path, passing under the mitral valve. The biological valve shows a strong jet with a peak velocity about twice as high compared to all mechanical heart valves, which makes it easier to penetrate deeply into the cavity. Accordingly, the peak kinetic energy in the left ventricle in case of the biological valve is about four times higher than the mechanical heart valves. We conclude that the tomographic particle imaging velocimetry setup provides a useful ground truth measurement of flow features and allows a comparison of the effects of different valve types on left ventricular flow patterns.

1 Introduction

The left ventricle (LV) is believed to preserve the momentum of the incoming blood flow during diastole by keeping it in motion during diastasis and smoothly redirecting it towards the outflow tract during systole (Kim et al. 1995; Kilner et al. 2000). The topology of these flow structures is determined by the geometry of the LV cavity, the morphology of the mitral valve and the electrical conduction system (Bermejo et al. 2015; Mele et al. 2018). Various multidisciplinary studies have

been conducted to better understand the pathophysiology of heart disease, to define clinically useful indicators of cardiac function (Gharib et al. 2006; Belohlavek 2012) and/or to understand the effect of mitral valve repair or replacement by a prosthetic device on the LV flow (V Vraghav , Sudeep Sastry 2018). The choice of a biological vs. mechanical prosthesis for instance is still an open debate (Chikwe 2018) as shown in a recent observational study by (Goldstone 2017).

Particle image velocimetry (PIV) has been extensively used to study the effect of different prosthetic valves on the LV flow pattern (Pierrakos et al. 2004; Kheradvar et al. 2006; Querzoli and Fortini 2010; Falahatpisheh and Kheradvar 2012; Vukićević et al. 2012; Wang et al. 2017). A common limitation of these PIV studies is their 2D approach, yielding an incomplete view of the inherently three-dimensional (3D) flow structures in the LV and the inability to calculate all nine components of the velocity gradient tensor. There have been various attempts to overcome this limitation by reconstructing the 3D velocity vector field in the whole LV from velocity data obtained from separate measurement planes. The latter are either two-component velocity (Fortini et al. 2013; Falahatpisheh et al. 2014b) or three-component velocity data, obtained by the stereoscopic PIV technique (Tan et al. 2016; Saaid et al. 2018). Both reconstructive methods take advantage of the periodicity of the cardiac cycle but require complex setups to translate or rotate the PIV system as well as time-consuming calibration and/or post processing procedures.

Tomographic PIV (Tomo-PIV) is considered the first “true” volumetric PIV technique (Elsinga et al. 2005). In contrast to traditional planar PIV techniques, Tomo-PIV allows instantaneous extraction of all three velocity components over the entire volume of interest. To date, Tomo-PIV has been used for studying the blood flow in the aortic root (Hasler et al. 2016; Hasler and Obrist 2018), the carotid artery (Buchmann et al. 2011) and the intracranial aneurysm (Roloff et al. 2018).

Considering the above, the goal of the following work is twofold. First, we aim to demonstrate the feasibility of a tomographic, full-volumetric PIV technique to capture the 3D flow in a realistic and compliant LV model. Additionally, this phantom is compatible with 3D ultrasound and MRI imaging, such that 3D flow measurements acquired by these in-vivo medical imaging approaches can be compared to the optical ground truth in the future. Second, we compare the flow field generated by three structurally different prosthetic heart valves (biological, tilting disc and bileaflet) under the same running conditions.

2 Materials and Methods

2.1 Left ventricle membrane and tank

An optically transparent compliant silicone LV replica (0.5 mm thick) (Fig 1b) was manufactured by painting four layers of silicone (HT 33 Transparent LT, Zhermack SpA, Rome, Italy) onto a 3D

printed LV mould (Fig 1a). The shape of the LV mould was extracted from the statistical mean of a dataset of segmented 4D computed tomography images of 150 patients (Kirişli et al. 2010; Metz et al. 2012; Voorneveld et al. 2018). The silicone has a refractive index of 1.413, measured by an Abbe refractometer (Bleeker, Zeist Holland).

The LV membrane was connected to the valve holders (Fig 1c), and immersed (Fig 1d) in a Plexiglas nine-sided polygon tank (Fig 2a). The Plexiglas plates were machined and then glued together using a two-component reaction adhesive (Acrifix 192, Evonic Industries). Fig. 2a depicts the LV flow loop, which consists of a pressurized aortic chamber and an atrial chamber kept at atmospheric pressure. The outlet from the aortic chamber is connected to the left atrial chamber via an adjustable peripheral resistance valve (Vivitro Labs Inc., Victoria, BC, Canada) with a short length of silicone rubber hose.

2.2 Hydraulic circuit

A pulsatile pump (Vivitro Labs Inc., BC, Canada) was used to mimic the pumping action of the LV. The hydraulic piston pump was connected to the acrylic tank (Fig 2a) with semi-rigid tubing. The pump was velocity-controlled and set to generate a sinusoidal-like waveform with a frequency of 70 beats per minute and a duty cycle of 35%, resulting in a 300 ms systolic period and a stroke volume of 50 ml. Pressure transducers (6069, Utah Medical Products, Inc., Athlone, Ireland) were used to monitor the pressure in the aorta and inside the tank.

2.3 Imaging system and illumination

The imaging system consists of two high-speed cameras (Imager Pro HS 4M, PCO, Kelheim, Germany) set to record at 2000 fps. The setup was primarily designed to perform tomographic PIV from four different viewing angles using two cameras (Fig 3a). For this purpose, a custom-made image splitter (consisting of 8 first surface mirrors) has been placed in front of each camera (Fig 3a). Macro prime lenses with a focal length of 100 mm (Samyang Optics co Ltd., Korea) were used. A long-pass filter at 540 nm (Thorlabs, Inc., Newton, NJ, USA) was mounted in front of each lens to selectively capture the scattered fluorescent particle light. A volume of approximately $80 \times 110 \times 70$ mm^3 was illuminated by a double-cavity pulsed Nd:YLF laser (527 nm Litron Laser, England). Diverging lenses were used to shape the laser beam into a full-volume illumination.

2.4 Working fluid and tracer particles

A two-component working fluid was chosen to match the measured refractive index (1.4130) of the LV silicone membrane, thereby minimizing optical distortion. The ratio of the components in the fluid mixture (60% glycerol and 40% distilled water) was adjusted until its measured refractive index

(1.4140) very closely matched that of the silicone. The dynamic viscosity and density of the working fluid were 17.7 mPa·s and 1160 kg/m^3, respectively. Fluorescent Rhodamine-B coated particles with a diameter of 20-50 μm and density of 1100 kg/m^3 were used as tracers.

2.5 Calibration

A two-level calibration target was placed with a micrometre stage in nine positions equally spaced over 40 mm in the tank (without the LV membrane). To map the 3D space object onto the 2D camera sensor plane, a third-order polynomial fitting method was applied. The geometrical calibration yielded an average error for all cameras and views of approximately 0.2 pixel. Subsequently, an ensemble of 200 particle images has been acquired to perform the iterative volume self-calibration procedure (Wieneke 2008). After four iterations, the volume self- calibration was able to reduce the disparity to less than 0.02 pixels for all cameras.

2.6 Tomographic analysis

All particle images were pre-processed to remove background intensity with a 7×7 sliding minimum kernel. Due to the Gaussian laser illumination shape, an intensity normalization filter was applied. Subsequent image processing involves 3×3 Gaussian smoothing, successive sharpening and manually masking out the non-flow regions. Following the suggested particle concentration from literature (Scarano 2012) a concentration of 0.04 particles per pixel (PPP) was reached as an optimal measurement condition. The time separation Δt of 500 μs between image pairs was optimized to ensure that maximum particle displacement is about 6-10 pixels. All tomographic PIV data were processed with Davis 10 (LaVision, Göttingen, Germany).

2.7 Measurement protocol

The measurements were performed within the LV with three different heart valves mounted in the mitral position (Fig 4a): a 25 mm tricuspid biological, a 24 mm tilting disc and a 25 mm Bicarbon bileaflet valve which was mounted in two different orientations (anatomic and anti-anatomic). In all series a 19 mm Perimount Magna Ease (Edwards Lifesciences) tricuspid biological valve was used as an aortic valve. The particle images were reconstructed at 61 time points over the cardiac cycle (temporal resolution of 14 ms). The data from ten cardiac cycles were phase-averaged for each heart valve configuration. Table 1, summarizing the relevant setup and processing parameters, is provided as a supplementary material.

3 Results and discussion

In the following, the Tomo-PIV phase-averaged velocity data are presented. The first subsection illustrates the mean flow velocity field downstream of the four prosthetic valves. Further, we focus on the inflow characteristics by comparing the flow rate through transversal slices over time. In the last two subsections, we present the vortical structures and kinetic energy computed in the entire LV domain.

Fig 4b compares the maximum inlet flow velocity between the four valves. The biological valve (BHV) opens slightly later than the mechanical valves (MHVs) and the transmitral flow velocity increases more rapidly for the BHV, reaching a peak value of up to 1 m/s - twice the magnitude of the MHVs. At the onset of the diastole, the tilting disc produces slightly higher velocities than the two bileaflet configurations. The two orientations of the bileaflet valve yielded virtually identical inlet velocities throughout diastole.

3.1 Flow Velocity field

A note of caution is necessary, because of the large difference in the flow velocity range between the biological and mechanical valves (Fig 4b), different colour scales were used for the iso-surfaces and velocity maps (Fig 5). Fig. 5 shows the mean flow topology of the tested heart valves (indicated with letters) at four characteristic phases (indicated with Roman numerals) during the cardiac cycle. The flow topology is represented by means of iso-surfaces based on the velocity magnitude and cross-sectional slices coloured with axial velocity.

Biological valve: Initially, a strong transmitral jet is directed towards the anterior LV wall (time steps I-II). By the end of diastole (time step III), the inner core of the inflow starts disappearing (high velocity isosurface). Further, the inflow swirls towards the posterior wall, forming a counter-rotating flow pattern occupying the entire cavity. This flow feature is believed to prevent blood stasis by washing-out the apical region. The outgoing flow slides along the posterior wall and then crosses the inflow tract (time step IV). The crossed flow path shown here with the BHV (dashed line Fig 5) agrees with previous in vivo studies (Pierrakos et al. 2004; Faludi et al. 2010; Pedrizzetti et al. 2010; Akiyama et al. 2017; Nakashima et al. 2017), where the flow passing the BHV was shown to generate a strong jet towards the intraventricular septum and then to cross the inflow path (i.e. passing under the mitral valve) during systole (Fig 5a).

Monoleaflet valve: At the onset of the filling phase (time step I) the valve induces a primary jet passing the main orifice. The primary jet advances along the posterior wall, while a secondary jet passes from the anterior orifice towards the anterior wall (time step II). At the end of diastole, the incoming flow forms a clockwise large-scale vortex (time step III) that is smoothly redirected towards

the outflow tract. This looped flow path is in concordance with previous 2D-PIV investigations (Cenedese et al. 2005; Vukićević et al. 2012; Voorneveld et al. 2018; Khalafvand et al. 2018).

Bileaflet valve: The two valve orientations exhibit minor differences in flow topology at the onset of the filling phase (Fig 5c-d): in both cases the jet emanating from the outer orifices is significantly stronger than in the central orifice (time steps I-II). In the anatomic configuration (Fig 5c), the jet on the anterior wall septum rolls off under the aortic valve, whereas due to the "Coandă effect" the opposite jet tends to realign with the central inflow jet (time steps II-III). In the anti-anatomic orientation (Fig 5d), on the other hand, the flow pattern through the outer orifices appears to be nearly symmetric (time steps II-III). In both configurations, at mid diastole the strong central jet merges with the outer jets towards the apex. The iso-velocity surface emanating from the mitral valve dissipates before reaching the apex (Fig 5c-d), as previously described in (Pierrakos et al. 2004). Additionally, our results indicate that in both configurations the bileaflet valve gives rise to a crossed flow path. This confirms the findings from a prior in vivo study from (Faludi et al. 2010). Conversely, (Nakashima et al. 2017), using an ultrasound based vector flow mapping technique, showed that only the anti-anatomical orientation is associated with a crossed flow path. In our previous work (Saaid et al. 2018), we even observed that both orientations lead to a looped flow path. Some of the discrepancies may be due to the highly simplified LV shape and the different LV diameter/valve ratio (Saaid et al. 2018) or a limitation of two-dimensional echocardiography in case of (Nakashima et al. 2017). Movie 1 (online supplement) depicts the flow field throughout one cardiac cycle for each valve model.

3.2 Inflow characteristics

For a more quantitative comparison between the BHV and the MHVs, the volume flow rate has been calculated through four cross-sections (Fig 6) over one cardiac cycle. As shown in figure 6 (cross-section 1), the three mechanical valves open simultaneously. The two bileaflet orientations behave similarly in the first slices with a slightly higher flow rate than the biological and the tilting disc valves during the diastole. Moving towards the apex, in cross-sections 3 and 4, the penetration depth of the jet decreases drastically in the MHVs. In fact, the BHV exhibits a much higher downward flow over the filling phase compared to the bileaflet valve in anatomic configuration (cross-section 4). The stagnation phenomena in a LV have also been reported in a 2D-PIV investigation by Faludi and co-workers (Faludi et al. 2010), showing that the jet entering the LV cavity collides more closely to the apex with a biological valve than with a bileaflet valve. Compared to the MHVs, the inflow jet through the BHV is more likely to reach and wash out the apical region. This potentially avoids stagnation zones and reduces the risk for thrombosis formation. In patients with dilated cardiomyopathy or myocardial infarction, where abnormal flow patterns are known to promote blood stasis between the apex and outflow tract (Dantzig 1995; Sengupta et al. 2008; Hendabadi et al. 2013), we would expect the BHV to perform better than the MHVs.

205

206 ### 3.3 Vortical structures

207 The lambda-2 (λ_2) method has been used to identify the 3D vortical flow features over the cardiac
208 cycle (Jeong and Hussain 1995). In figure 7, one can clearly see the formation of the vortex rings (time
209 step I) and observe how they elongate, propagate and then dissipate during diastole. The strong inflow
210 through the biological valve develops as a single vortex ring in the shear layer around the incoming jet
211 (time steps I-II-III). The primary vortex ring is connected to a secondary vortex via branched tubes
212 (trailing vortex tubes). The two vortices travel towards the mid-ventricle and start to break down in
213 small structures before reaching the apex. The described vortex ring formation downstream the BHV
214 is somewhat similar to the vortices generated from a cylinder with an inclined exit (Troolin and
215 Longmire 2010). Comparable flow structures have also been described in previous LV fluid dynamic
216 simulations (Watanabe et al. 2008; Le and Sotiropoulos 2012; Khalafvand et al. 2019) and in vivo
217 studies (Elbaz et al. 2014).

218 The three MHVs exhibited different vortical flow features compared with the BHV. In case of the
219 tilting disc, the flow through the posterior orifice yields a strong shear layer and interacted with the
220 boundary layer along the lateral wall generating a curved vortex ring (Fig 7b). The vortical structures
221 then shed from the valve leaflets, progress toward the mid regions, and finally dissipate by the end of
222 the diastole due to viscous interaction with the ventricular wall.

223 Due to the leaflet geometry of the bileaflet valve, the inflow is spread over multiple orifices, rendering
224 the formation of a single vortex impossible. Thus, the bileaflet valve induces incomplete vortex rings
225 through the three orifices (Fig 7c-d). At the onset of the filling phase, the flow is dominated by tubular
226 structures generated from the outer orifices. Further into diastole (time step IV), a jet is formed from
227 the central orifice with higher propagation velocity, forming a concentric coherent structure. The latter
228 interact rapidly with each other and with the surrounding LV wall, disintegrating into smaller flow
229 structures. Additionally, the so-called vortex ring was observed only downstream the biological valve
230 with the formation of multiple vortex rings. The complete evolution of the vortical flow structures past
231 the prosthetic heart valves over the cardiac cycle is provided as a supplementary material (movie 2).

232

233 #### 3.4 Kinetic energy

234 The time course of integral kinetic energy (KE) computed for the entire LV domain is shown in figure
235 8. The peak value of the kinetic energy passing the BHV is approximately four times higher than for
236 the MHVs, as could be expected from the two-fold difference in the velocity magnitude profile during
237 the cardiac cycle (Fig 4). A significant difference in terms of KE between BHV and bileaflet valve has
238 been also reported in a recent numerical study by (Meschini et al. 2018). All mechanical valves exhibit

a similarly shaped KE profile throughout the cardiac cycle. The tilting disc lead to higher KE levels during mid diastole and systole than did the bileaflet valve. In case of the bileaflet valve, the anatomic orientation yielded a slightly higher KE than the anti-anatomic configuration.

3.5 Limitations

Despite the aforementioned advantages of the employed technique, some limitations are worthwhile mentioning. Tomo-PIV hardware and software are generally more complex and expensive than 2D PIV or multiplane scanning setups. However, to reduce the cost of the PIV apparatus, a four-view Tomo-PIV imaging system has been implemented using a combination of only two cameras (instead of four) and a mirror system. Also, while Tomo-PIV does not require physical alignment between illumination and the calibration target, it is more sensitive to vibrations compared to stereoscopic PIV, which may lead to camera misalignment during the acquisition. To overcome this, we followed a well-established procedure for physical calibration, followed by the volume-self calibration. Due to computational cost and amount of data storage, we have presented only the averaged flow field data based on 10 cycles. A semi-quantitative convergence analysis (consisting of a comparison between the phase averaged data obtained from 10, 20 and 30 cycles) showed no discernible difference between 20 and 30 cycles. Only at peak early inflow a 7% difference in flow velocity was found between the results obtained with 10 cycles and the converged flow velocity data using 30 cycles. Moreover, we would like to mention that more advanced Lagrangian software algorithms, such as Shake-The-Box (Schanz et al. 2016), may be more appropriate to analyse the time-resolved data in the future. Furthermore, the piston pump was driven by a sinusoidal-like wave form that does not represent diastasis and the late filling (A-wave). Consequently, it was not possible to investigate the interaction between the flow structures induced at the early filling and the fresh fluid entering during the late filling wave, as described in vivo (Elbaz et al. 2014) and in a recent numerical simulation study (Khalafvand et al. 2018), using a similar LV geometry and a more realistic flow waveform. Also, the working fluid mixture has a dynamic viscosity four times higher than blood, which may have affected the flow resistance and consequently the formation and viscous dissipation rate of the vortical structures.

4 Conclusion

This work demonstrated the feasibility and usefulness of tomographic PIV, to study 3D flow dynamics in a compliant model. To the best of our knowledge, this study provides the first tomographic PIV study of the 3D flow pattern in a flexible left ventricular shape membrane, downstream of biological and mechanical valves.

We have analysed the effect of three types of prosthetic mitral heart valves on intraventricular flow under the same hydraulic conditions. The qualitative and quantitative flow analyses suggest that the biological valve generates flow patterns similar to those observed in vivo after a BHV valve replacement. Except for the tilting disc, all tested prosthetic valves induced a crossed flow path, where the outflow crosses the inflow path, passing under the mitral valve. Further, the inflow jet in the BHV penetrated deeper into the LV cavity compared to the MHVs. The lambda-2 method for vortex identification showed the formation of multiple vortex rings in the presence of the BHV. The kinetic energy level associated with the BHV during diastole is approximately four times higher than the MHVs. Finally, we showed that the anatomic orientation of the bileaflet valve yields an overall slightly higher kinetic energy than the anti-anatomic configuration. Yet, none of our performed analyses reveal that one orientation of the bileaflet valve is to be preferred over the other.

Acknowledgements

We acknowledge Michiel Manten and Geert Springeling of Erasmus Medical Center, for their assistance in fabricating the phantom. This work was supported in part by ZonMw within the Innovative Medical Devices Initiative (IMDI) program (project Heart Failure and 4D Flow)

Conflict of interest statement

All authors declare that there are no conflicts of interest.

References

Akiyama K, Nakamura N, Itatani K, et al (2017) Flow-dynamics assessment of mitral-valve surgery by intraoperative vector flow mapping. 24:869–875. doi: 10.1093/icvts/ivx033

Belohlavek M (2012) Vortex formation time: An emerging echocardiographic index of left ventricular filling efficiency? Eur Heart J Cardiovasc Imaging 13:367–369. doi: 10.1093/ejechocard/jer311

Bermejo J, Martínez-Legazpi P, del Álamo JC (2015) The Clinical Assessment of Intraventricular Flows. Annu Rev Fluid Mech 47:315–342. doi: 10.1146/annurev-fluid-010814-014728

Buchmann NA, Atkinson C, Jeremy MC, Soria J (2011) Tomographic particle image velocimetry investigation of the flow in a modeled human carotid artery bifurcation. Exp Fluids 50:1131–1151. doi: 10.1007/s00348-011-1042-1

Cenedese A, Del Prete Z, Miozzi M, Querzoli G (2005) A laboratory investigation of the flow in the left ventricle of a human heart with prosthetic, tilting-disk valves. Exp Fluids 39:322–335. doi: 10.1007/s00348-005-1006-4

Chikwe (2018) Prosthesis Type for Aortic- and Mitral-Valve Replacement. N Engl J Med 776–779.

304 doi: 10.1056/NEJMc1715189

305 Dantzig JM Van (1995) Doppler Left Ventricular Flow Pattern Versus Conventional Predictors of Left
306 Ventricular Thrombus After Acute Myocardial Infarction. 25:1341–1346. doi: 10.1016/0735-
307 1097(94)00548-5

308 Elbaz MSM, Calkoen EE, Westenberg JJM, et al (2014) Vortex flow during early and late left
309 ventricular filling in normal subjects: quantitative characterization using retrospectively-gated
310 4D flow cardiovascular magnetic resonance and three-dimensional vortex core analysis. J
311 Cardiovasc Magn Reson 16:78. doi: 10.1186/s12968-014-0078-9

312 Elsinga GE, Scarano F, Wieneke B, van Oudheusden BW (2005) Tomographic particle image
313 velocimetry. 6th Int Symp Part Image Velocim 1–12.

314 Falahatpisheh A, Kheradvar A (2012) High-speed particle image velocimetry to assess cardiac fluid
315 dynamics in vitro: From performance to validation. Eur J Mech B/Fluids 35:2–8. doi:
316 10.1016/j.euromechflu.2012.01.019

317 Falahatpisheh A, Pedrizzetti G, Kheradvar A (2014) Three-dimensional reconstruction of cardiac
318 flows based on multi-planar velocity fields. Exp Fluids. doi: 10.1007/s00348-014-1848-8

319 Faludi R, Szulik M, D'hooge J, et al (2010) Left ventricular flow patterns in healthy subjects and
320 patients with prosthetic mitral valves: An in vivo study using echocardiographic particle image
321 velocimetry. J Thorac Cardiovasc Surg 139:1501–1510. doi: 10.1016/j.jtcvs.2009.07.060

322 Fortini S, Querzoli G, Espa S, Cenedese a. (2013) Three-dimensional structure of the flow inside the
323 left ventricle of the human heart. Exp Fluids. doi: 10.1007/s00348-013-1609-0

324 Gharib M, Rambod E, Kheradvar A, et al (2006) Optimal vortex formation as an index of cardiac
325 health. Proc Natl Acad Sci U S A 103:6305–6308. doi: 10.1073/pnas.0600520103

326 Goldstone (2017) Mechanical or Biologic Prostheses for Aortic-Valve and Mitral-Valve Replacement.
327 1847–1857. doi: 10.1056/NEJMoa1613792

328 Hasler D, Landolt A, Obrist D (2016) Tomographic PIV behind a prosthetic heart valve. Exp Fluids
329 57:1–13. doi: 10.1007/s00348-016-2158-0

330 Hasler D, Obrist D (2018) Three-dimensional flow structures past a bio- prosthetic valve in an in-vitro
331 model of the aortic root.

332 Hendabadi SAH, Ermejo JAB, Enito YOB, et al (2013) Topology of Blood Transport in the Human
333 Left Ventricle by Novel Processing of Doppler Echocardiography. 41:2603–2616. doi:
334 10.1007/s10439-013-0853-z

335 Jeong J, Hussain F (1995) On the identification of a vortex. J Fluid Mech 285:69. doi:
336 10.1017/S0022112095000462

337 Khalafvand SS, Voorneveld JD, Muralidharan A, et al (2018) Assessment of human left ventricle flow
338 using statistical shape modelling and computational fluid dynamics. J Biomech 74:116–125. doi:
339 10.1016/j.jbiomech.2018.04.030

340 Khalafvand SS, Xu F, Westenberg J, et al (2019) Intraventricular blood fl ow with a fully dynamic
341 mitral valve model. Comput Biol Med 104:197–204. doi: 10.1016/j.compbiomed.2018.11.024

342 Kilner PJ, Yang G, Wilkes AJ, et al (2000) Asymmetric redirection of flow through the heart. 759–
343 761.

344 Kim WY, Walker PG, Pedersen EM, et al (1995) Left ventricular blood flow patterns in normal
345 subjects: A quantitative analysis by three-dimensional magnetic resonance velocity mapping. J
346 Am Coll Cardiol 26:224–238. doi: 10.1016/0735-1097(95)00141-L

347 Kirişli HA, Schaap M, Klein S (2010) Evaluation of a multi-atlas based method for segmentation of
348 cardiac CTA data : a large-scale , multicenter , and multivendor study. Am Assoc Phys Med
349 6279–6291. doi: 10.1118/1.3512795

350 Le TB, Sotiropoulos F (2012) On the three-dimensional vortical structure of early diastolic flow in a
351 patient-specific left ventricle. Eur J Mech B/Fluids 35:20–24. doi:
352 10.1016/j.euromechflu.2012.01.013

353 Mele D, Smarrazzo V, Pedrizzetti G, et al (2018) Intracardiac Flow Analysis : Techniques and
354 Potential Clinical Applications. J Am Soc Echocardiogr. doi: 10.1016/j.echo.2018.10.018

355 Meschini V, Tullio MD De, Querzoli G, Verzicco R (2018) Flow structure in healthy and pathological
356 left ventricles with natural and prosthetic mitral valves. 271–307. doi: 10.1017/jfm.2017.725

357 Metz CT, Baka N, Kirisli H, et al (2012) Regression-Based Cardiac Motion Prediction. IEEE Trans
358 Med Imaging 31:1311–1325.

359 Nakashima K, Itatani K, Kitamura T, Oka N (2017) Energy dynamics of the intraventricular vortex
360 after mitral valve surgery. Heart Vessels 0:0. doi: 10.1007/s00380-017-0967-6

361 Okafor IU, Santhanakrishnan A, Chaffins BD, et al (2015) Cardiovascular magnetic resonance
362 compatible physical model of the left ventricle for multi-modality characterization of wall
363 motion and hemodynamics. J Cardiovasc Magn Reson 17:51. doi: 10.1186/s12968-015-0154-9

364 Pedrizzetti GIP, Omenichini FED, Tonti GT (2010) On the Left Ventricular Vortex Reversal after
365 Mitral Valve Replacement. Ann Biomed Eng 38:769–773. doi: 10.1007/s10439-010-9928-2

Pierrakos O, Vlachos PP, Telionis DP (2004) Time-resolved DPIV analysis of vortex dynamics in a left ventricular model through bileaflet mechanical and porcine heart valve prostheses. J Biomech Eng 126:714–726. doi: 10.1115/1.1824124

Querzoli G, Fortini S (2010) Effect of the prosthetic mitral valve on vortex dynamics and turbulence of the left ventricular flow. doi: 10.1063/1.3371720

Roloff C, Stucht D, Beuing O, Berg P (2018) Comparison of intracranial aneurysm flow quantification techniques : standard PIV vs stereoscopic PIV vs tomographic PIV vs phase- contrast MRI vs CFD. 1–8. doi: 10.1136/neurintsurg-2018-013921

Saaid H, Segers P, Novara M, et al (2018) Single calibration multiplane stereo-PIV : the effect of mitral valve orientation on three-dimensional flow in a left ventricle model. Exp Fluids 59:1–13. doi: 10.1007/s00348-018-2504-5

Scarano F (2012) Tomographic PIV: principles and practice. Meas Sci Technol 24:012001. doi: 10.1088/0957-0233/24/1/012001

Sengupta PP, Burke R, Khandheria BK, Belohlavek M (2008) Following the Flow in Chambers. Heart Fail Clin 4:325–332. doi: 10.1016/j.hfc.2008.02.005

Tan SG-D, Kim S, Hon JKF, Leo HL (2016) A D-Shaped Bileaflet Bioprosthesis which Replicates Physiological Left Ventricular Flow Patterns. PLoS One 11:e0156580. doi: 10.1371/journal.pone.0156580

Troolin DR, Longmire EK (2010) Volumetric velocity measurements of vortex rings from inclined exits. Exp Fluids 48:409–420. doi: 10.1007/s00348-009-0745-z

V Vraghav , Sudeep Sastry NS (2018) Experimental Assessment of Flow Fields Associated with Heart Valve Prostheses Using Particle Image Velocimetry (PIV): Recommendations for Best Practices. 9:273–287. doi: 10.1007/s13239-018-0348-z

Voorneveld J., Muralidharan A., Hope T., Vos H. J., Kruizinga P., van der Steen A. F. W., Gijsen F. J. H., Kenjeres S. de JN and BJG (2018) High Frame Rate Ultrasound Particle Image Velocimetry for Estimating High Velocity Flow Patterns in the Left Ventricle. IEEE Trans Ultrason Ferroelectr Freq Control PP:1. doi: 10.1109/TUFFC.2017.2786340

Vukićević M, Fortini S, Querzoli G, et al (2012) Experimental study of an asymmetric heart valve prototype. Eur J Mech B/Fluids 35:54–60. doi: 10.1016/j.euromechflu.2012.01.014

Wang J, Gao Q, Wei R, Wang J (2017) Experimental study on the effect of an artificial cardiac valve on the left ventricular flow. Exp Fluids 58:126. doi: 10.1007/s00348-017-2409-8

Watanabe H, Sugiura S, Hisada T (2008) The looped heart does not save energy by maintaining the

momentum of blood flowing in the ventricle. AJP Hear Circ Physiol 294:H2191–H2196. doi: 10.1152/ajpheart.00041.2008

Wieneke B (2008) Volume self-calibration for 3D particle image velocimetry. Exp Fluids 549–556. doi: 10.1007/s00348-008-0521-5

Figure Legends

Fig. 1. (a) 3D-printed LV mould representing *the endocardial shape at end systole,* fitted with a mitral inflow and aortic outflow tract. (b) LV silicone membrane. (c) LV model attached to valve holders using cable ties. The outflow tract is tilted about 40° with respect to the mitral valve axis. (d) A long exposure picture of fluorescent particles within the LV.

Fig. 2. (a) CAD view of the nine-sided tank. The shape of the tank provides undistorted optical access to the LV from different angles. *W indicates the four windows used for optical access. The red arrows depict the LV flow loop*. 1-2: valve holders, 3-4: mitral and aortic valve position, 5-6: atrial and aortic blocks, 7: aortic pressure catheter, 8: multiple hose connectors for air removal and ventricular pressure monitoring, 9: pump connector. (b) Representative samples of ventricular pressure recorded during the PIV experiments and flow waveforms imposed at the pump.

Fig. 3. (a) Schematic sketch (top view) of the tomo-PIV setup. (b) Picture of tomo-PIV setup in linear configuration with two high-speed cameras equipped with prime lenses and filter (1), two mirror splitter system (2) and laser arm with telescopic head and optics compound (3). The nine-sided tank (4), with atrial (5) and aortic blocks (6), connected with peripheral resistance (7). Pressure transducer tubes (8). The tank is connected to the pulsatile pump via a semi-flexible tube (9).

Fig. 4. (a) Snapshots of the LV model and heart valves in the mitral position: (1) biological Perimount 2900 (Edwards Lifesciences, Irvine, USA); (2) tilting disk (Björk-Shiley); (3-4) bileaflet (Sorin Biomedica, Saluggia, Italy) in anatomic and anti-anatomic orientation, respectively. (b) peak velocity of the inflow jet during the diastolic phase.

Fig. 5. Time-sequence of the mean flow structures downstream of the mitral valves: (a) biological, (b) tilting disc, and bileaflet in (c) anatomic and (d) anti-anatomic orientation. Note that (d) is slightly rotated about the y-axis to improve visibility of the flow structures. Two iso-velocity surfaces are shown for each valve (at 0.35 m/s and 0.75 m/s in case of the BHV and at 0.15 m/s and 0.35 m/s in case of the MHVs). *On the right, a sketch of the LV and prosthetic valve showing the flow path (looped or crossed) with a dashed line*. The cross-sections are colour-coded based on the axial velocity (v_y). Roman numerals indicate the time steps (I = 0.35s, II = 0.55s, III = 0.8s, IV = 0.2s).

Fig. 6. Left: Four equidistant (20 mm) cross-sections within the LV model. The first slice is positioned approximately 5 mm below the mitral valve. Right: Volume flow rate computed through four cross-sections for each valve. Only the downward flow was considered; velocities with a positive sign (v_y) were blanked. The MHVs open approximately at 0.54s whereas the biological open at 0.58s.

Fig. 7. 3D vortical structures recognized by lambda-2 method are visualized as iso-surface (λ_2 = -0.015) and colour-coded with the axial velocity component. The 2D velocity vector field maps are coloured based on vorticity magnitude. (a) Biological, (b) tilting disc, and bileaflet in anatomic (c) and anti-anatomic (d) orientation. Roman numerals indicate the time steps (I=0.35s, II=0.45s, III=0.55s, IV=0.65s, V=0.85s).

Fig. 8. Left: the evolution of the kinetic energy within the LV domain, computed over the cardiac cycle as: $KE = 0.5\rho \int V^2 dv$, where $\rho = 1060\, kg/m^3$ and V is velocity magnitude. *Right: The difference of KE in the biological valve relative to each of the mechanical valves, calculated as:* $100\% * (BHV - MHV_i)/MHV_i$

Figure 1

Click here to download high resolution image

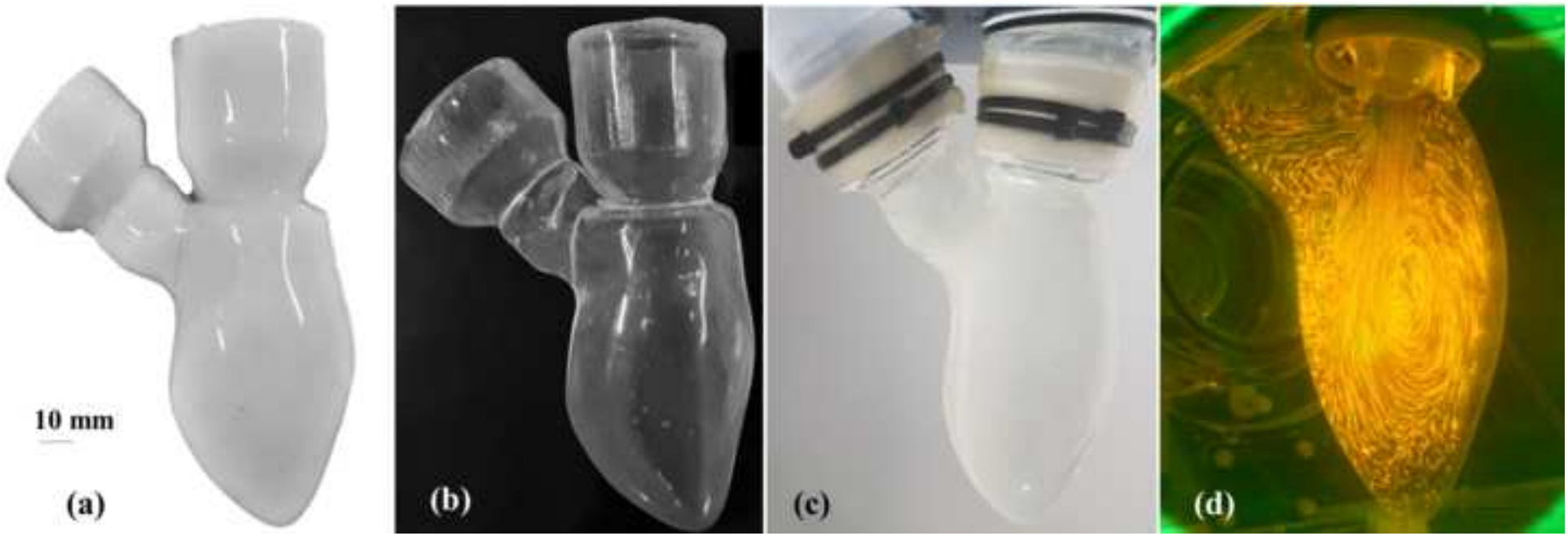

Figure 2

Click here to download high resolution image

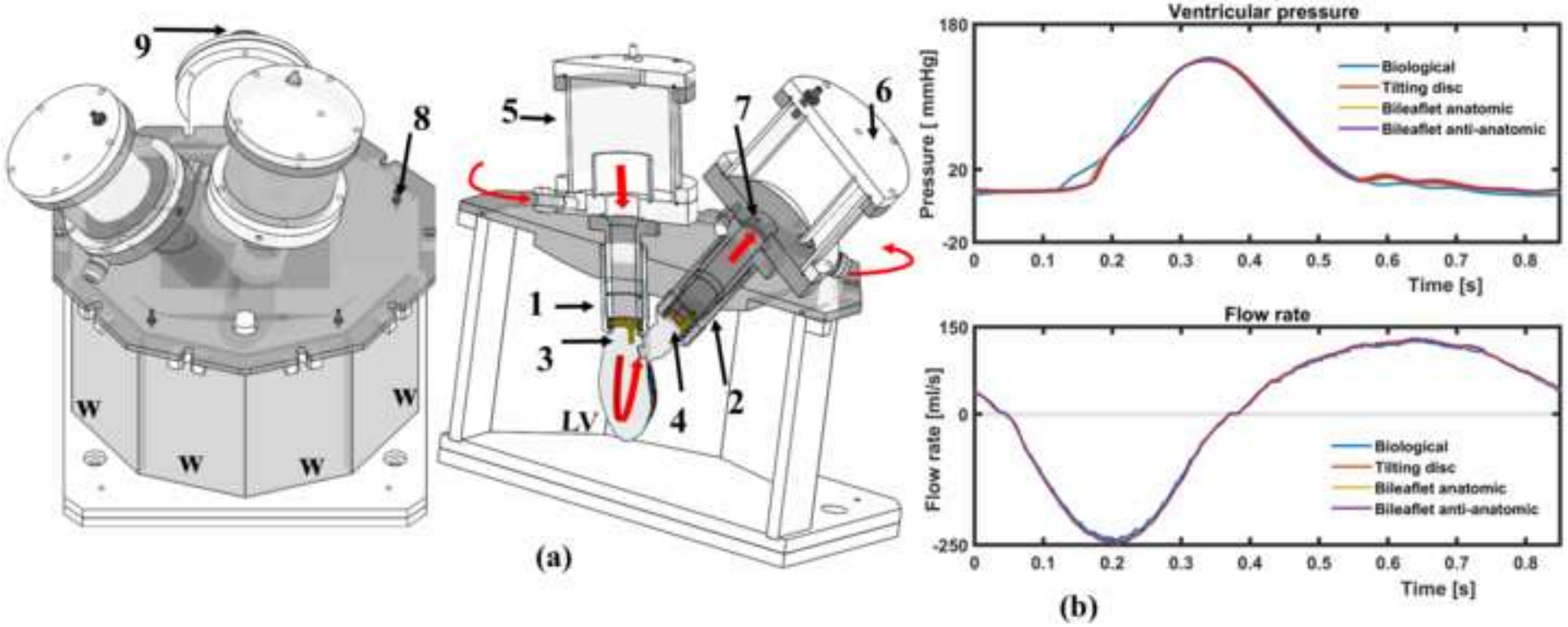

Figure 3

Click here to download high resolution image

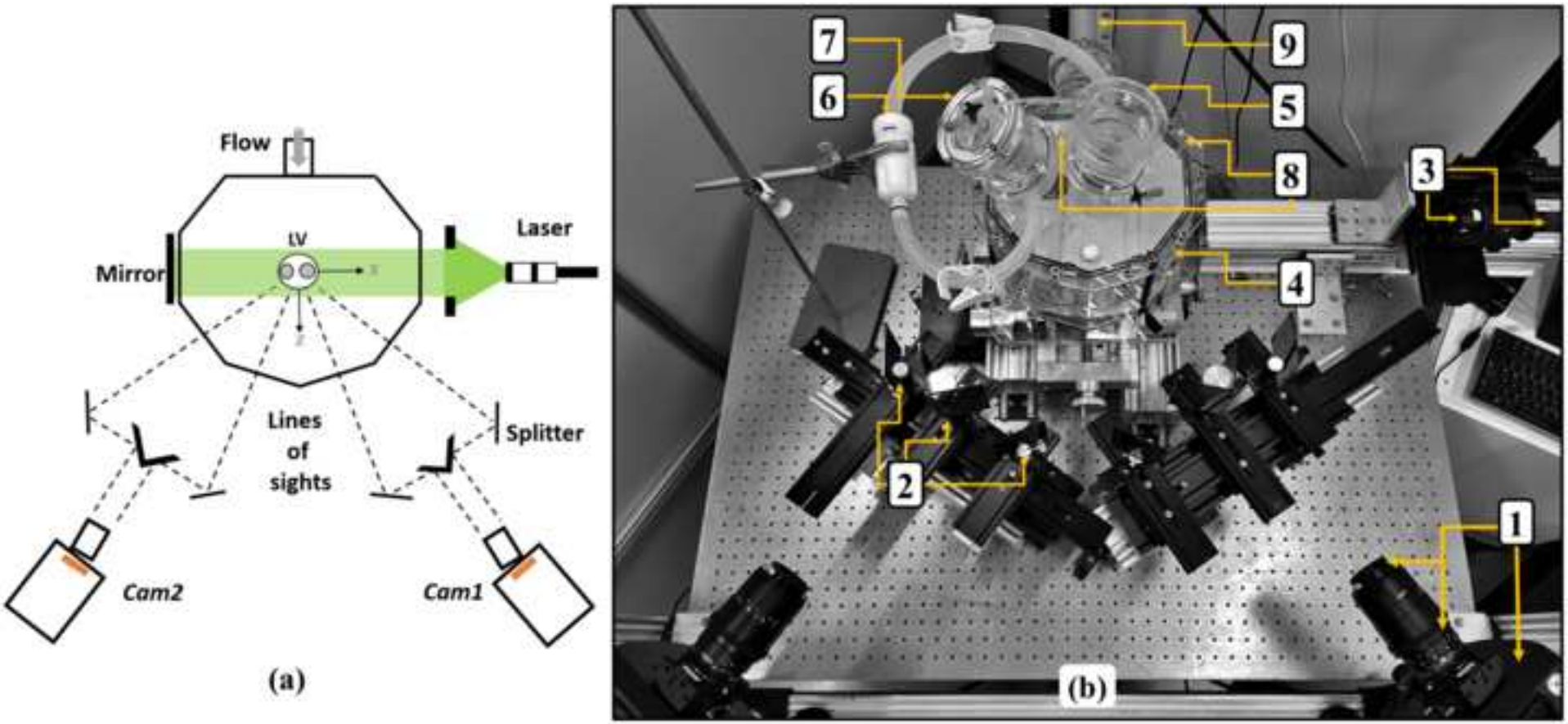

Figure 4

Click here to download high resolution image

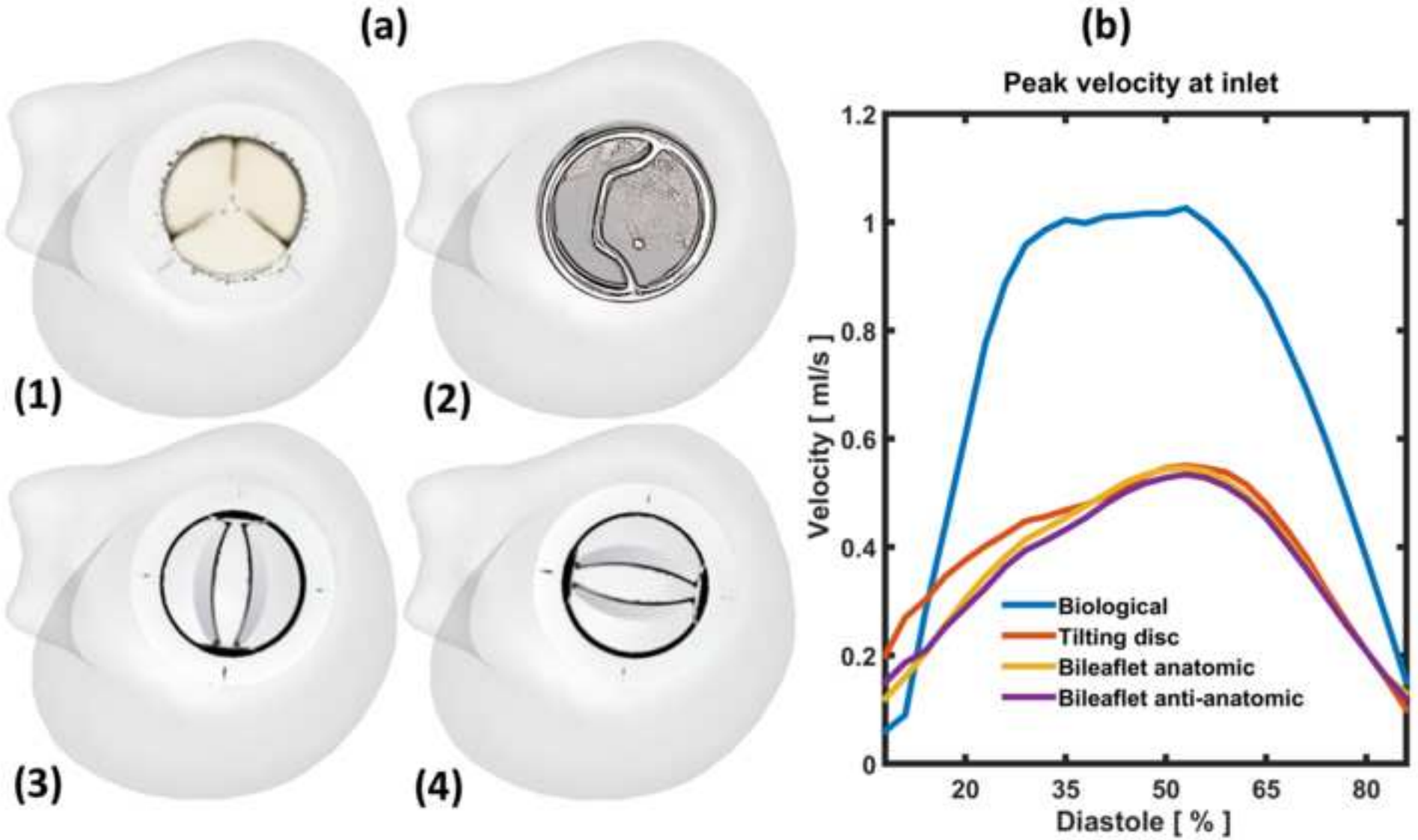

Figure 5

Click here to download high resolution image

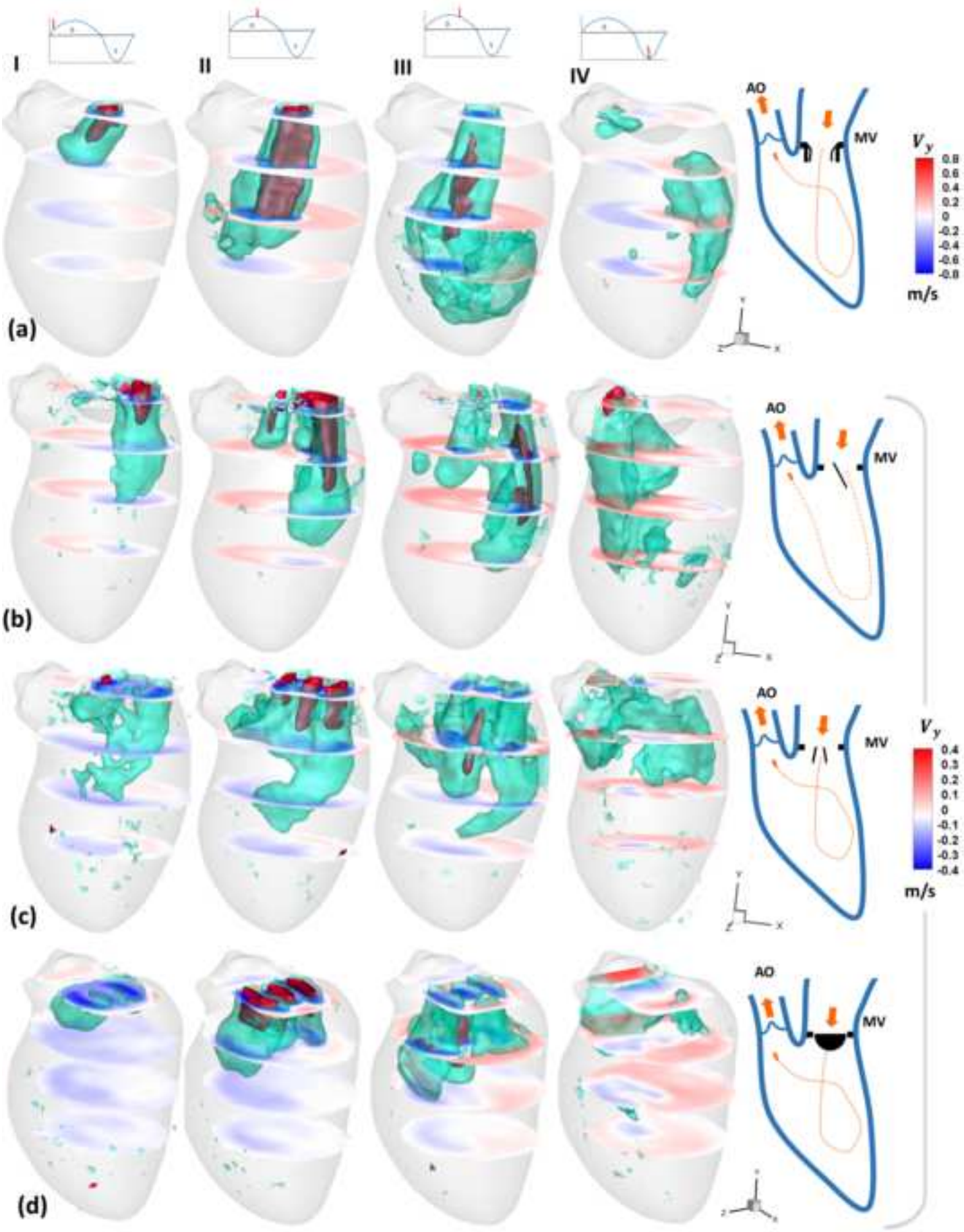

Figure 6

Click here to download high resolution image

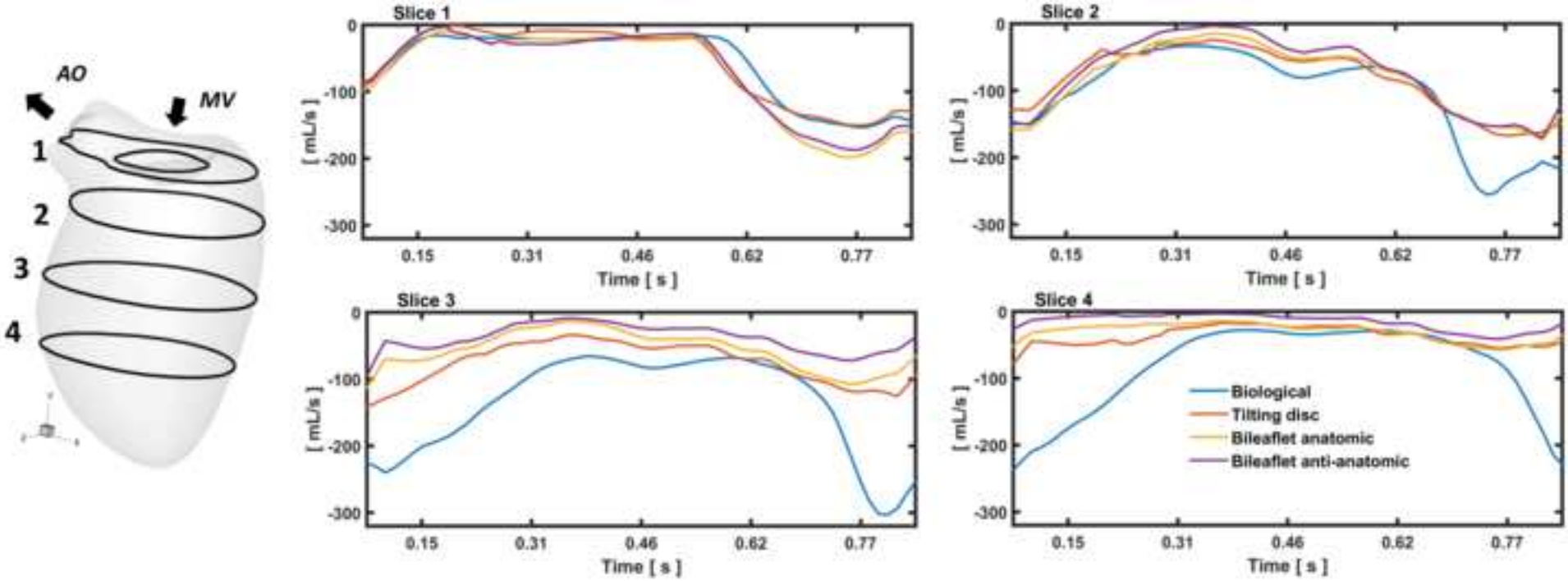

Figure 7

Click here to download high resolution image

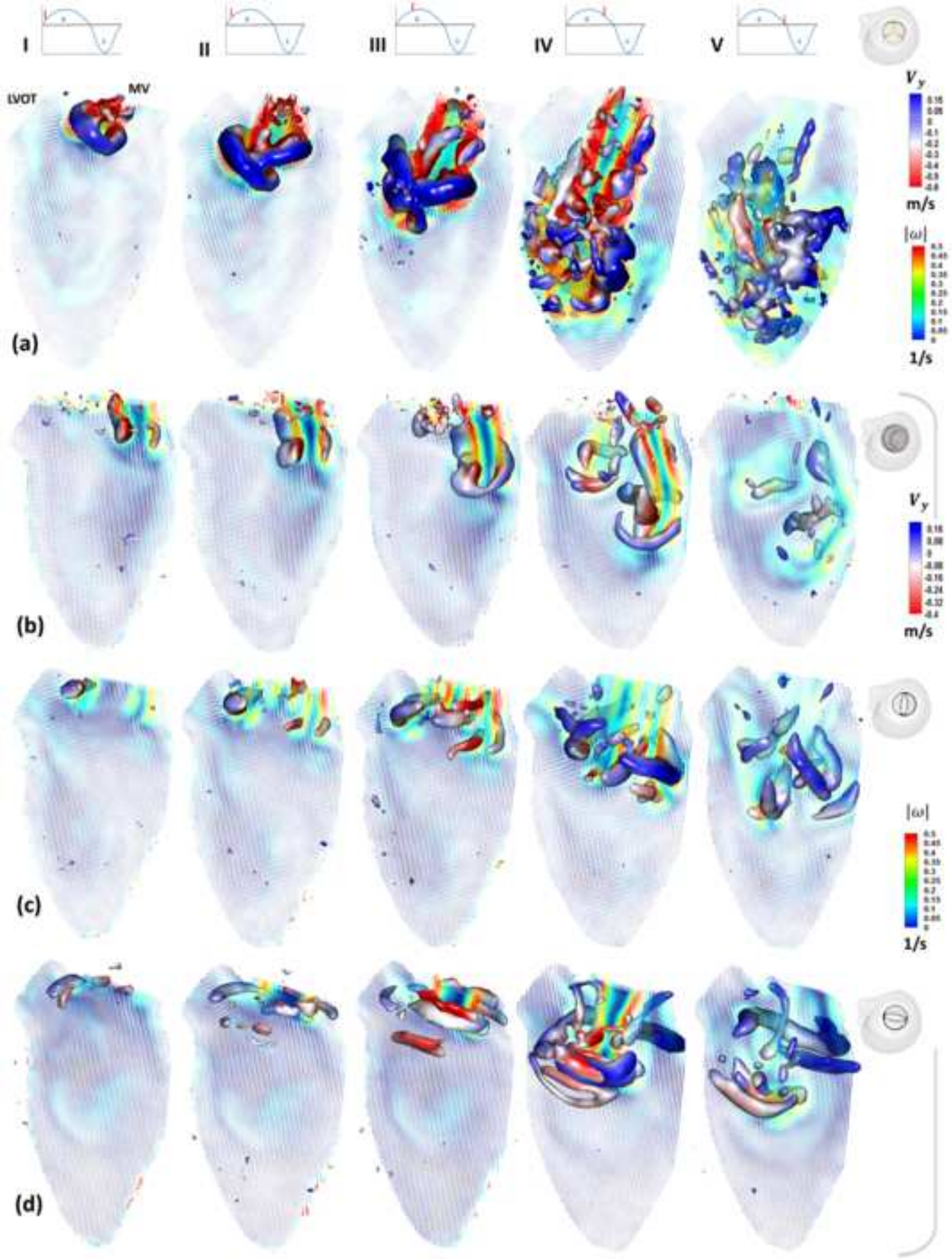

Figure 8

Click here to download high resolution image

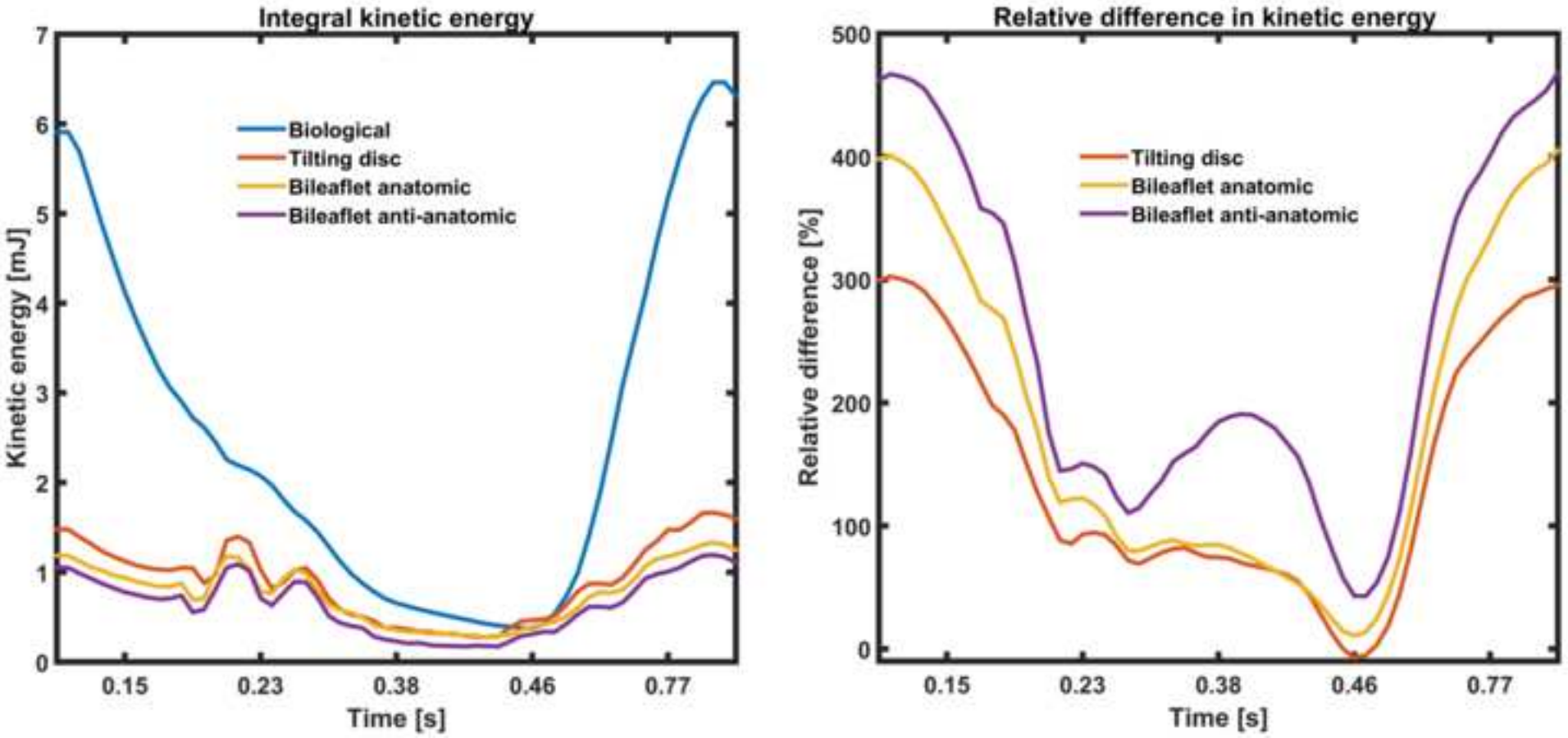

Tomographic PIV in a Model of the Left Ventricle: 3D Flow Past Biological and Mechanical Heart Valves

Hicham Saaid[1], Jason Voorneveld[2], Christiaan Schinkel[3], Jos Westenberg[4], Frank Gijsen[2], Patrick Segers[1], Pascal Verdonck[1], Nico de Jong[2], Johan G. Bosch[2], Sasa Kenjeres[3], Tom Claessens[5]

1 Institute Biomedical Technology, Ghent University, Ghent, Belgium

2 Department of Biomedical Engineering, Thoraxcenter, Erasmus MC University Medical Center, Rotterdam, The Netherlands

3 Department of Chemical Engineering, Faculty of Applied Sciences, Delft University of Technology, Delft, The Netherlands

4 Department of Radiology, Leiden University Medical Center, Leiden, The Netherlands

5 Department of Materials, Textiles and Chemical Engineering, Ghent University, Ghent, Belgium

Abstract

Left ventricular flow is intrinsically complex, three-dimensional and unsteady. Its features are susceptible to cardiovascular pathology and treatment, in particular to surgical interventions involving the valves (mitral valve replacement). To improve our understanding of intraventricular fluid mechanics and the impact of various types of prosthetic valves thereon, we have developed a custom-designed versatile left ventricular phantom with anatomically realistic moving left ventricular membrane. A biological, a tilting disc and a bileaflet valve (in two different orientations) were mounted in the mitral position and tested under the same settings. To investigate 3D flow within the phantom, a four-view tomographic particle image velocimetry setup has been implemented. The results compare side-by-side the evolution of the 3D flow topology, vortical structures and kinetic energy in the left ventricle domain during the cardiac cycle. Except for the tilting disc valve, all tested prosthetic valves induced a crossed flow path, where the outflow crosses the inflow path, passing under the mitral valve. The biological valve shows a strong jet with a peak velocity about twice as high compared to all mechanical heart valves, which makes it easier to penetrate deeply into the cavity. Accordingly, the peak kinetic energy in the left ventricle in case of the biological valve is about four times higher than the mechanical heart valves. We conclude that the tomographic particle imaging velocimetry setup provides a useful ground truth measurement of flow features and allows a comparison of the effects of different valve types on left ventricular flow patterns.

1 Introduction

The left ventricle (LV) is believed to preserve the momentum of the incoming blood flow during diastole by keeping it in motion during diastasis and smoothly redirecting it towards the outflow tract during systole (Kim et al. 1995; Kilner et al. 2000). The topology of these flow structures is determined by the geometry of the LV cavity, the morphology of the mitral valve and the electrical conduction system (Bermejo et al. 2015; Mele et al. 2018). Various multidisciplinary studies have

been conducted to better understand the pathophysiology of heart disease, to define clinically useful indicators of cardiac function (Gharib et al. 2006; Belohlavek 2012) and/or to understand the effect of mitral valve repair or replacement by a prosthetic device on the LV flow (V Vraghav , Sudeep Sastry 2018). *The choice of a biological vs. mechanical prosthesis for instance is still an open debate (Chikwe 2018) as shown in a recent observational study by (Goldstone 2017).*

Particle image velocimetry (PIV) has been extensively used to study the effect of different prosthetic valves on the LV flow pattern (Pierrakos et al. 2004; Kheradvar et al. 2006; Querzoli and Fortini 2010; Falahatpisheh and Kheradvar 2012; Vukićević et al. 2012; Wang et al. 2017). A common limitation of these PIV studies is their 2D approach, yielding an incomplete view of the inherently three-dimensional (3D) flow structures in the LV and the inability to calculate all nine components of the velocity gradient tensor. There have been various attempts to overcome this limitation by reconstructing the 3D velocity vector field in the whole LV from velocity data obtained from separate measurement planes. The latter are either two-component velocity (Fortini et al. 2013; Falahatpisheh et al. 2014b) or three-component velocity data, obtained by the stereoscopic PIV technique (Tan et al. 2016; Saaid et al. 2018). Both reconstructive methods take advantage of the periodicity of the cardiac cycle but require complex setups to translate or rotate the PIV system as well as time-consuming calibration and/or post processing procedures.

Tomographic PIV (Tomo-PIV) is considered the first "true" volumetric PIV technique (Elsinga et al. 2005). In contrast to traditional planar PIV techniques, Tomo-PIV allows instantaneous extraction of all three velocity components over the entire volume of interest. *To date, Tomo-PIV has been used for studying the blood flow in the aortic root (Hasler et al. 2016; Hasler and Obrist 2018), the carotid artery (Buchmann et al. 2011) and the intracranial aneurysm (Roloff et al. 2018).*

Considering the above, the goal of the following work is twofold. First, we aim to demonstrate the feasibility of a tomographic, full-volumetric PIV technique to capture the 3D flow in a realistic and compliant LV model. *Additionally, this phantom is compatible with 3D ultrasound and MRI imaging, such that 3D flow measurements acquired by these in-vivo medical imaging approaches can be compared to the optical ground truth in the future.* Second, we compare the flow field generated by three structurally different prosthetic heart valves (biological, tilting disc and bileaflet) under the same running conditions.

2 Materials and Methods

2.1 Left ventricle membrane and tank

An optically transparent compliant silicone LV replica (0.5 mm thick) (Fig 1b) was manufactured by painting four layers of silicone (HT 33 Transparent LT, Zhermack SpA, Rome, Italy) onto a 3D

printed LV mould (Fig 1a). The shape of the LV mould was extracted from the statistical mean of a dataset of segmented 4D computed tomography images *of 150 patients* (Kirişli et al. 2010*;* Metz et al. 2012; Voorneveld et al. 2018). The silicone has a refractive index of 1.413, measured by an Abbe refractometer (Bleeker, Zeist Holland).

The LV membrane was connected to the valve holders (Fig 1c), and immersed (Fig 1d) in a Plexiglas nine-sided polygon tank (Fig 2a). The Plexiglas plates were machined and then glued together using a two-component reaction adhesive (Acrifix 192, Evonic Industries). Fig. 2a depicts the LV flow loop, which consists of a pressurized aortic chamber and an atrial chamber kept at atmospheric pressure. *The outlet from the aortic chamber is connected to the left atrial chamber via an adjustable peripheral resistance valve (Vivitro Labs Inc., Victoria, BC, Canada) with a short length of silicone rubber hose.*

2.2 Hydraulic circuit

A pulsatile pump (Vivitro Labs Inc., BC, Canada) was used to mimic the pumping action of the LV. The hydraulic piston pump was connected to the acrylic tank (Fig 2a) with semi-rigid tubing. The pump was velocity-controlled and set to generate a sinusoidal-like waveform with a frequency of 70 beats per minute and a duty cycle of 35%, resulting in a 300 ms systolic period and a stroke volume of 50 ml. Pressure transducers (6069, Utah Medical Products, Inc., Athlone, Ireland) were used to monitor the pressure in the aorta and inside the tank.

2.3 Imaging system and illumination

The imaging system consists of two high-speed cameras (Imager Pro HS 4M, PCO, Kelheim, Germany) set to record at 2000 fps. The setup was primarily designed to perform tomographic PIV from four different viewing angles using two cameras (Fig 3a). For this purpose, a custom-made image splitter (consisting of 8 first surface mirrors) has been placed in front of each camera (Fig 3a). Macro prime lenses with a focal length of 100 mm (Samyang Optics co Ltd., Korea) were used. A long-pass filter at 540 nm (Thorlabs, Inc., Newton, NJ, USA) was mounted in front of each lens to selectively capture the scattered fluorescent particle light. A volume of approximately 80×110×70 mm^3 was illuminated by a double-cavity pulsed Nd:YLF laser (527 nm Litron Laser, England). Diverging lenses were used to shape the laser beam into a full-volume illumination.

2.4 Working fluid and tracer particles

A two-component working fluid was chosen to match the measured refractive index (1.4130) of the LV silicone membrane, thereby minimizing optical distortion. *The ratio of the components in the fluid mixture (60% glycerol and 40% distilled water) was adjusted until its measured refractive index*

(1.4140) very closely matched that of the silicone. The dynamic viscosity and density of the working fluid were 17.7 mPa·s and 1160 kg/m^3, respectively. Fluorescent Rhodamine-B coated particles with a diameter of 20-50 µm and density of 1100 kg/m^3 were used as tracers.

2.5 Calibration

A two-level calibration target was placed with a micrometre stage in nine positions equally spaced over 40 mm in the tank (without the LV membrane). To map the 3D space object onto the 2D camera sensor plane, a third-order polynomial fitting method was applied. The geometrical calibration yielded an average error for all cameras and views of approximately 0.2 pixel. Subsequently, an ensemble of 200 particle images has been acquired to perform the iterative volume self-calibration procedure (Wieneke 2008). After four iterations, the volume self- calibration was able to reduce the disparity to less than 0.02 pixels for all cameras.

2.6 Tomographic analysis

All particle images were pre-processed to remove background intensity with a 7×7 sliding minimum kernel. Due to the Gaussian laser illumination shape, an intensity normalization filter was applied. Subsequent image processing involves 3×3 Gaussian smoothing, successive sharpening and manually masking out the non-flow regions. Following the suggested particle concentration from literature (Scarano 2012) a concentration of 0.04 particles per pixel (PPP) was reached as an optimal measurement condition. The time separation Δt of 500 µs between image pairs was optimized to ensure that maximum particle displacement is about 6-10 pixels. All tomographic PIV data were processed with Davis 10 (LaVision, Göttingen, Germany).

2.7 Measurement protocol

The measurements were performed within the LV with three different heart valves mounted in the mitral position (Fig 4a): a 25 mm tricuspid biological, a 24 mm tilting disc and a 25 mm Bicarbon bileaflet valve which was mounted in two different orientations (anatomic and anti-anatomic). In all series a 19 mm Perimount Magna Ease (Edwards Lifesciences) tricuspid biological valve was used as an aortic valve. The particle images were reconstructed at 61 time points over the cardiac cycle (temporal resolution of 14 ms). The data from ten cardiac cycles were phase-averaged for each heart valve configuration. Table 1, summarizing the relevant setup and processing parameters, is provided as a supplementary material.

3 Results and discussion

In the following, the Tomo-PIV phase-averaged velocity data are presented. The first subsection illustrates the mean flow velocity field downstream of the four prosthetic valves. Further, we focus on the inflow characteristics by comparing the flow rate through transversal slices over time. In the last two subsections, we present the vortical structures and kinetic energy computed in the entire LV domain.

Fig 4b compares the maximum inlet flow velocity between the four valves. The biological valve (BHV) opens slightly later than the mechanical valves (MHVs) and the transmitral flow velocity increases more rapidly for the BHV, reaching a peak value of up to 1 m/s - twice the magnitude of the MHVs. At the onset of the diastole, the tilting disc produces slightly higher velocities than the two bileaflet configurations. The two orientations of the bileaflet valve yielded virtually identical inlet velocities throughout diastole.

3.1 Flow Velocity field

A note of caution is necessary, because of the large difference in the flow velocity range between the biological and mechanical valves (Fig 4b), different colour scales were used for the iso-surfaces and velocity maps (Fig 5). Fig. 5 shows the mean flow topology of the tested heart valves (indicated with letters) at four characteristic phases (indicated with Roman numerals) during the cardiac cycle. The flow topology is represented by means of iso-surfaces based on the velocity magnitude and cross-sectional slices coloured with axial velocity.

Biological valve: Initially, a strong transmitral jet is directed towards the anterior LV wall (time steps I-II). By the end of diastole (time step III), the inner core of the inflow starts disappearing (high velocity isosurface). Further, the inflow swirls towards the posterior wall, forming a counter-rotating flow pattern occupying the entire cavity. This flow feature is believed to prevent blood stasis by washing-out the apical region. The outgoing flow slides along the posterior wall and then crosses the inflow tract (time step IV). The crossed flow path shown here with the BHV (dashed line Fig 5) agrees with previous *in vivo* studies (Pierrakos et al. 2004; Faludi et al. 2010; Pedrizzetti et al. 2010; Akiyama et al. 2017; Nakashima et al. 2017), where the flow passing the BHV was shown to generate a strong jet towards the intraventricular septum and then to cross the inflow path (i.e. passing under the mitral valve) during systole (Fig 5a).

Monoleaflet valve: At the onset of the filling phase (time step I) the valve induces a primary jet passing the main orifice. The primary jet advances along the posterior wall, while a secondary jet passes from the anterior orifice towards the anterior wall (time step II). At the end of diastole, the incoming flow forms a clockwise large-scale vortex (time step III) that is smoothly redirected towards

the outflow tract. This looped flow path is in concordance with previous 2D-PIV investigations (Cenedese et al. 2005; Vukićević et al. 2012; Voorneveld et al. 2018; Khalafvand et al. 2018).

Bileaflet valve: The two valve orientations exhibit minor differences in flow topology at the onset of the filling phase (Fig 5c-d): in both cases the jet emanating from the outer orifices is significantly stronger than in the central orifice (time steps I-II). In the anatomic configuration (Fig 5c), the jet on the anterior wall septum rolls off under the aortic valve, whereas due to the "Coandă effect" the opposite jet tends to realign with the central inflow jet (time steps II-III). *In the anti-anatomic orientation (Fig 5d), on the other hand, the flow pattern through the outer orifices appears to be nearly symmetric (time steps II-III)*. In both configurations, at mid diastole the strong central jet merges with the outer jets towards the apex. The iso-velocity surface emanating from the mitral valve dissipates before reaching the apex (Fig 5c-d), as previously described in (Pierrakos et al. 2004). *Additionally, our results indicate that in both configurations the bileaflet valve gives rise to a crossed flow path. This confirms the findings from a prior in vivo study from (Faludi et al. 2010). Conversely,* (Nakashima et al. 2017), *using an ultrasound based vector flow mapping technique, showed that only the anti-anatomical orientation is associated with a crossed flow path. In our previous work (Saaid et al. 2018), we even observed that both orientations lead to a looped flow path. Some of the discrepancies may be due to the highly simplified LV shape and the different LV diameter/valve ratio (Saaid et al. 2018) or a limitation of two-dimensional echocardiography in case of (Nakashima et al. 2017).* Movie 1 (online supplement) depicts the flow field throughout one cardiac cycle for each valve model.

3.2 Inflow characteristics

For a more quantitative comparison between the BHV and the MHVs, the volume flow rate has been calculated through four cross-sections (Fig 6) over one cardiac cycle. As shown in figure 6 (cross-section 1), the three mechanical valves open simultaneously. The two bileaflet orientations behave similarly in the first slices with a slightly higher flow rate than the biological and the tilting disc valves during the diastole. Moving towards the apex, in cross-sections 3 and 4, the penetration depth of the jet decreases drastically in the MHVs. In fact, the BHV exhibits a much higher downward flow over the filling phase compared to the bileaflet valve in anatomic configuration (cross-section 4). The stagnation phenomena in a LV have also been reported in a 2D-PIV investigation by Faludi and co-workers (Faludi et al. 2010), showing that the jet entering the LV cavity collides more closely to the apex with a biological valve than with a bileaflet valve. *Compared to the MHVs, the inflow jet through the BHV is more likely to reach and wash out the apical region. This potentially avoids stagnation zones and reduces the risk for thrombosis formation. In patients with dilated cardiomyopathy or myocardial infarction, where abnormal flow patterns are known to promote blood stasis between the*

apex and outflow tract (Dantzig 1995; Sengupta et al. 2008; Hendabadi et al. 2013), we would expect the BHV to perform better than the MHVs.

3.3 Vortical structures

The lambda-2 (λ_2) method has been used to identify the 3D vortical flow features over the cardiac cycle (Jeong and Hussain 1995). In figure 7, one can clearly see the formation of the vortex rings (time step I) and observe how they elongate, propagate and then dissipate during diastole. The strong inflow through the biological valve develops as a single vortex ring in the shear layer around the incoming jet (time steps I-II-III). The primary vortex ring is connected to a secondary vortex via branched tubes (trailing vortex tubes). The two vortices travel towards the mid-ventricle and start to break down in small structures before reaching the apex. The described vortex ring formation downstream the BHV is somewhat similar to the vortices generated from a cylinder with an inclined exit (Troolin and Longmire 2010). Comparable flow structures have also been described in previous LV fluid dynamic simulations (Watanabe et al. 2008; Le and Sotiropoulos 2012; Khalafvand et al. 2019) and *in vivo* studies (Elbaz et al. 2014).

The three MHVs exhibited different vortical flow features compared with the BHV. In case of the tilting disc, the flow through the posterior orifice yields a strong shear layer and interacted with the boundary layer along the lateral wall generating a curved vortex ring (Fig 7b). The vortical structures then shed from the valve leaflets, progress toward the mid regions, and finally dissipate by the end of the diastole due to viscous interaction with the ventricular wall.

Due to the leaflet geometry of the bileaflet valve, the inflow is spread over multiple orifices, rendering the formation of a single vortex impossible. Thus, the bileaflet valve induces incomplete vortex rings through the three orifices (Fig 7c-d). At the onset of the filling phase, the flow is dominated by tubular structures generated from the outer orifices. Further into diastole (time step IV), a jet is formed from the central orifice with higher propagation velocity, forming a concentric coherent structure. The latter interact rapidly with each other and with the surrounding LV wall, disintegrating into smaller flow structures. Additionally, the so-called vortex ring was observed only downstream the biological valve with the formation of multiple vortex rings. The complete evolution of the vortical flow structures past the prosthetic heart valves over the cardiac cycle is provided as a supplementary material (movie 2).

3.4 Kinetic energy

The time course of integral kinetic energy (KE) computed for the entire LV domain is shown in figure 8. The peak value of the kinetic energy passing the BHV is approximately four times higher than for

the MHVs, as could be expected from the two-fold difference in the velocity magnitude profile during the cardiac cycle (Fig 4). A significant difference in terms of KE between BHV and bileaflet valve has been also reported in a recent numerical study by (Meschini et al. 2018). All mechanical valves exhibit a similarly shaped KE profile throughout the cardiac cycle. The tilting disc lead to higher KE levels during mid diastole and systole than did the bileaflet valve. In case of the bileaflet valve, the anatomic orientation yielded a slightly higher KE than the anti-anatomic configuration.

3.5 Limitations

Despite the aforementioned advantages of the employed technique, some limitations are worthwhile mentioning. *Tomo-PIV hardware and software are generally more complex and expensive than 2D PIV or multiplane scanning setups. However, to reduce the cost of the PIV apparatus, a four-view Tomo-PIV imaging system has been implemented using a combination of only two cameras (instead of four) and a mirror system. Also, while Tomo-PIV does not require physical alignment between illumination and the calibration target, it is more sensitive to vibrations compared to stereoscopic PIV, which may lead to camera misalignment during the acquisition. To overcome this, we followed a well-established procedure for physical calibration, followed by the volume-self calibration.* Due to computational cost and amount of data storage, we have presented only the averaged flow field data *based on 10 cycles. A semi-quantitative convergence analysis (consisting of a comparison between the phase averaged data obtained from 10, 20 and 30 cycles) showed no discernible difference between 20 and 30 cycles. Only at peak early inflow a 7% difference in flow velocity was found between the results obtained with 10 cycles and the converged flow velocity data using 30 cycles.* Moreover, we would like to mention that more advanced Lagrangian software algorithms, such as Shake-The-Box (Schanz et al. 2016), may be more appropriate to analyse the time-resolved data in the future. Furthermore, the piston pump was driven by a sinusoidal-like wave form that does not represent diastasis and the late filling (A-wave). *Consequently, it was not possible to investigate the interaction between the flow structures induced at the early filling and the fresh fluid entering during the late filling wave, as described in vivo (Elbaz et al. 2014) and in a recent numerical simulation study (Khalafvand et al. 2018), using a similar LV geometry and a more realistic flow waveform. Also, the working fluid mixture has a dynamic viscosity four times higher than blood, which may have affected the flow resistance and consequently the formation and viscous dissipation rate of the vortical structures.*

4 Conclusion

This work demonstrated the feasibility and usefulness of tomographic PIV, to study 3D flow dynamics in a compliant model. To the best of our knowledge, this study provides the first tomographic PIV

study of the 3D flow pattern in a flexible left ventricular shape membrane, downstream of biological and mechanical valves.

We have analysed the effect of three types of prosthetic mitral heart valves on intraventricular flow under the same hydraulic conditions. The qualitative and quantitative flow analyses suggest that the biological valve generates flow patterns similar to those observed in vivo after a BHV valve replacement. Except for the tilting disc, all tested prosthetic valves induced a crossed flow path, where the outflow crosses the inflow path, passing under the mitral valve. Further, the inflow jet in the BHV penetrated deeper into the LV cavity compared to the MHVs. The lambda-2 method for vortex identification showed the formation of multiple vortex rings in the presence of the BHV. The kinetic energy level associated with the BHV during diastole is approximately four times higher than the MHVs. *Finally, we showed that the anatomic orientation of the bileaflet valve yields an overall slightly higher kinetic energy than the anti-anatomic configuration. Yet, none of our performed analyses reveal that one orientation of the bileaflet valve is to be preferred over the other*.

Acknowledgements

We acknowledge Michiel Manten and Geert Springeling of Erasmus Medical Center, for their assistance in fabricating the phantom. This work was supported in part by ZonMw within the Innovative Medical Devices Initiative (IMDI) program (project Heart Failure and 4D Flow)

Conflict of interest statement

All authors declare that there are no conflicts of interest.

References

Akiyama K, Nakamura N, Itatani K, et al (2017) Flow-dynamics assessment of mitral-valve surgery by intraoperative vector flow mapping. 24:869–875. doi: 10.1093/icvts/ivx033

Belohlavek M (2012) Vortex formation time: An emerging echocardiographic index of left ventricular filling efficiency? Eur Heart J Cardiovasc Imaging 13:367–369. doi: 10.1093/ejechocard/jer311

Bermejo J, Martínez-Legazpi P, del Álamo JC (2015) The Clinical Assessment of Intraventricular Flows. Annu Rev Fluid Mech 47:315–342. doi: 10.1146/annurev-fluid-010814-014728

Buchmann NA, Atkinson C, Jeremy MC, Soria J (2011) Tomographic particle image velocimetry investigation of the flow in a modeled human carotid artery bifurcation. Exp Fluids 50:1131–1151. doi: 10.1007/s00348-011-1042-1

Cenedese A, Del Prete Z, Miozzi M, Querzoli G (2005) A laboratory investigation of the flow in the left ventricle of a human heart with prosthetic, tilting-disk valves. Exp Fluids 39:322–335. doi:

10.1007/s00348-005-1006-4

Chikwe (2018) Prosthesis Type for Aortic- and Mitral-Valve Replacement. N Engl J Med 776–779. doi: 10.1056/NEJMc1715189

Dantzig JM Van (1995) Doppler Left Ventricular Flow Pattern Versus Conventional Predictors of Left Ventricular Thrombus After Acute Myocardial Infarction. 25:1341–1346. doi: 10.1016/0735-1097(94)00548-5

Elbaz MSM, Calkoen EE, Westenberg JJM, et al (2014) Vortex flow during early and late left ventricular filling in normal subjects: quantitative characterization using retrospectively-gated 4D flow cardiovascular magnetic resonance and three-dimensional vortex core analysis. J Cardiovasc Magn Reson 16:78. doi: 10.1186/s12968-014-0078-9

Elsinga GE, Scarano F, Wieneke B, van Oudheusden BW (2005) Tomographic particle image velocimetry. 6th Int Symp Part Image Velocim 1–12.

Falahatpisheh A, Kheradvar A (2012) High-speed particle image velocimetry to assess cardiac fluid dynamics in vitro: From performance to validation. Eur J Mech B/Fluids 35:2–8. doi: 10.1016/j.euromechflu.2012.01.019

Falahatpisheh A, Pedrizzetti G, Kheradvar A (2014) Three-dimensional reconstruction of cardiac flows based on multi-planar velocity fields. Exp Fluids. doi: 10.1007/s00348-014-1848-8

Faludi R, Szulik M, D'hooge J, et al (2010) Left ventricular flow patterns in healthy subjects and patients with prosthetic mitral valves: An in vivo study using echocardiographic particle image velocimetry. J Thorac Cardiovasc Surg 139:1501–1510. doi: 10.1016/j.jtcvs.2009.07.060

Fortini S, Querzoli G, Espa S, Cenedese a. (2013) Three-dimensional structure of the flow inside the left ventricle of the human heart. Exp Fluids. doi: 10.1007/s00348-013-1609-0

Gharib M, Rambod E, Kheradvar A, et al (2006) Optimal vortex formation as an index of cardiac health. Proc Natl Acad Sci U S A 103:6305–6308. doi: 10.1073/pnas.0600520103

Goldstone (2017) Mechanical or Biologic Prostheses for Aortic-Valve and Mitral-Valve Replacement. 1847–1857. doi: 10.1056/NEJMoa1613792

Hasler D, Landolt A, Obrist D (2016) Tomographic PIV behind a prosthetic heart valve. Exp Fluids 57:1–13. doi: 10.1007/s00348-016-2158-0

Hasler D, Obrist D (2018) Three-dimensional flow structures past a bio- prosthetic valve in an in-vitro model of the aortic root.

Hendabadi SAH, Ermejo JAB, Enito YOB, et al (2013) Topology of Blood Transport in the Human

Left Ventricle by Novel Processing of Doppler Echocardiography. 41:2603–2616. doi: 10.1007/s10439-013-0853-z

Jeong J, Hussain F (1995) On the identification of a vortex. J Fluid Mech 285:69. doi: 10.1017/S0022112095000462

Khalafvand SS, Voorneveld JD, Muralidharan A, et al (2018) Assessment of human left ventricle flow using statistical shape modelling and computational fluid dynamics. J Biomech 74:116–125. doi: 10.1016/j.jbiomech.2018.04.030

Khalafvand SS, Xu F, Westenberg J, et al (2019) Intraventricular blood fl ow with a fully dynamic mitral valve model. Comput Biol Med 104:197–204. doi: 10.1016/j.compbiomed.2018.11.024

Kilner PJ, Yang G, Wilkes AJ, et al (2000) Asymmetric redirection of flow through the heart. 759–761.

Kim WY, Walker PG, Pedersen EM, et al (1995) Left ventricular blood flow patterns in normal subjects: A quantitative analysis by three-dimensional magnetic resonance velocity mapping. J Am Coll Cardiol 26:224–238. doi: 10.1016/0735-1097(95)00141-L

Kirişli HA, Schaap M, Klein S (2010) Evaluation of a multi-atlas based method for segmentation of cardiac CTA data : a large-scale , multicenter , and multivendor study. Am Assoc Phys Med 6279–6291. doi: 10.1118/1.3512795

Le TB, Sotiropoulos F (2012) On the three-dimensional vortical structure of early diastolic flow in a patient-specific left ventricle. Eur J Mech B/Fluids 35:20–24. doi: 10.1016/j.euromechflu.2012.01.013

Mele D, Smarrazzo V, Pedrizzetti G, et al (2018) Intracardiac Flow Analysis : Techniques and Potential Clinical Applications. J Am Soc Echocardiogr. doi: 10.1016/j.echo.2018.10.018

Meschini V, Tullio MD De, Querzoli G, Verzicco R (2018) Flow structure in healthy and pathological left ventricles with natural and prosthetic mitral valves. 271–307. doi: 10.1017/jfm.2017.725

Metz CT, Baka N, Kirisli H, et al (2012) Regression-Based Cardiac Motion Prediction. IEEE Trans Med Imaging 31:1311–1325.

Nakashima K, Itatani K, Kitamura T, Oka N (2017) Energy dynamics of the intraventricular vortex after mitral valve surgery. Heart Vessels 0:0. doi: 10.1007/s00380-017-0967-6

Okafor IU, Santhanakrishnan A, Chaffins BD, et al (2015) Cardiovascular magnetic resonance compatible physical model of the left ventricle for multi-modality characterization of wall motion and hemodynamics. J Cardiovasc Magn Reson 17:51. doi: 10.1186/s12968-015-0154-9

Pedrizzetti GIP, Omenichini FED, Tonti GT (2010) On the Left Ventricular Vortex Reversal after Mitral Valve Replacement. Ann Biomed Eng 38:769–773. doi: 10.1007/s10439-010-9928-2

Pierrakos O, Vlachos PP, Telionis DP (2004) Time-resolved DPIV analysis of vortex dynamics in a left ventricular model through bileaflet mechanical and porcine heart valve prostheses. J Biomech Eng 126:714–726. doi: 10.1115/1.1824124

Querzoli G, Fortini S (2010) Effect of the prosthetic mitral valve on vortex dynamics and turbulence of the left ventricular flow. doi: 10.1063/1.3371720

Roloff C, Stucht D, Beuing O, Berg P (2018) Comparison of intracranial aneurysm flow quantification techniques : standard PIV vs stereoscopic PIV vs tomographic PIV vs phase- contrast MRI vs CFD. 1–8. doi: 10.1136/neurintsurg-2018-013921

Saaid H, Segers P, Novara M, et al (2018) Single calibration multiplane stereo-PIV : the effect of mitral valve orientation on three-dimensional flow in a left ventricle model. Exp Fluids 59:1–13. doi: 10.1007/s00348-018-2504-5

Scarano F (2012) Tomographic PIV: principles and practice. Meas Sci Technol 24:012001. doi: 10.1088/0957-0233/24/1/012001

Sengupta PP, Burke R, Khandheria BK, Belohlavek M (2008) Following the Flow in Chambers. Heart Fail Clin 4:325–332. doi: 10.1016/j.hfc.2008.02.005

Tan SG-D, Kim S, Hon JKF, Leo HL (2016) A D-Shaped Bileaflet Bioprosthesis which Replicates Physiological Left Ventricular Flow Patterns. PLoS One 11:e0156580. doi: 10.1371/journal.pone.0156580

Troolin DR, Longmire EK (2010) Volumetric velocity measurements of vortex rings from inclined exits. Exp Fluids 48:409–420. doi: 10.1007/s00348-009-0745-z

V Vraghav , Sudeep Sastry NS (2018) Experimental Assessment of Flow Fields Associated with Heart Valve Prostheses Using Particle Image Velocimetry (PIV): Recommendations for Best Practices. 9:273–287. doi: 10.1007/s13239-018-0348-z

Voorneveld J., Muralidharan A., Hope T., Vos H. J., Kruizinga P., van der Steen A. F. W., Gijsen F. J. H., Kenjeres S. de JN and BJG (2018) High Frame Rate Ultrasound Particle Image Velocimetry for Estimating High Velocity Flow Patterns in the Left Ventricle. IEEE Trans Ultrason Ferroelectr Freq Control PP:1. doi: 10.1109/TUFFC.2017.2786340

Vukićević M, Fortini S, Querzoli G, et al (2012) Experimental study of an asymmetric heart valve prototype. Eur J Mech B/Fluids 35:54–60. doi: 10.1016/j.euromechflu.2012.01.014

Wang J, Gao Q, Wei R, Wang J (2017) Experimental study on the effect of an artificial cardiac valve

on the left ventricular flow. Exp Fluids 58:126. doi: 10.1007/s00348-017-2409-8

Watanabe H, Sugiura S, Hisada T (2008) The looped heart does not save energy by maintaining the momentum of blood flowing in the ventricle. AJP Hear Circ Physiol 294:H2191–H2196. doi: 10.1152/ajpheart.00041.2008

Wieneke B (2008) Volume self-calibration for 3D particle image velocimetry. Exp Fluids 549–556. doi: 10.1007/s00348-008-0521-5

movie 1

Click here to download Supplementary Material: movie 1- Isosurfaces flow field.rar

movie 2

Click here to download Supplementary Material: movie 2 - vortex structures.rar

Table and notes

Click here to download Supplementary Material: Table 1 An overview on the most important parameters for the PIV system.docx

Conflict of interest statement

Saaid et al. Tomographic PIV in a Model of the Left Ventricle: 3D Flow Past Biological and Mechanical Heart Valves

All authors declare that there are no conflicts of interest of any type. This assertion is also included in the manuscript.